

EMRP SIB-05 DELIVERABLE 1.1.4

**SUMMARY REPORT OF PROPERTIES OF MATERIALS FOR
POTENTIAL USE AS MASS TRANSFER STANDARDS**

PAUL-ANDRÉ MEURY (LNE), DJILALI BENTOUATI (LNE), JAMES BERRY (NPL), STUART DAVIDSON (NPL), MARK PLIMMER (CNAM) ZACCARIA SILVESTRI (CNAM), MAIJA OJANEN (MIKES), RICHARD HOGSTROM (MIKES), PETER FUCHS (EJPD), KILIAN MARTI (EJPD), JAROSLAV ZUDA (CMI), SEVDA KACMAZ (UME), RICHARD GREEN (NRC)

JUNE 2015

EMRP SIB-05 DELIVERABLE 1.1.4

SUMMARY REPORT OF PROPERTIES OF MATERIALS FOR
POTENTIAL USE AS MASS TRANSFER STANDARDS

STUART DAVIDSON (NPL), JAMES BERRY (NPL)
Engineering Measurement Division

PAUL-ANDRÉ MEURY (LNE), DJILALI BENTOUATI (LNE),
MARK PLIMMER (CNAM) ZACCARIA SILVESTRI (CNAM),
MAIJA OJANEN (MIKES), RICHARD HOGSTROM (MIKES),
PETER FUCHS (EJPD), KILIAN MARTI (EJPD),
JAROSLAV ZUDA (CMI), SEVDA KACMAZ (UME),
RICHARD GREEN (NRC)

© Queen's Printer and Controller of HMSO, year 2015

ISSN 1754-2987

National Physical Laboratory
Hampton Road, Teddington, Middlesex, TW11 0LW

Extracts from this report may be reproduced provided the source is acknowledged
and the extract is not taken out of context.

Approved on behalf of NPLML by
Dr Andrew Lewis, Knowledge Leader, Engineering Measurement Division

1	INTRODUCTION	7
2	MATERIALS USED IN THE STUDY	7
3	TECHNIQUES USED	8
3.1	ATOMIC FORCE MICROSCOPY	8
3.2	SCANNING ELECTRON MICROSCOPY	8
3.3	ANGLE RESOLVED SCATTERING	8
3.4	WHITE LIGHT INTERFEROMETRY	10
3.5	X-RAY PHOTOELECTRON SPECTROSCOPY	10
3.6	X-RAY FLUORESCENCE	10
3.7	SPECTRAL ELLIPSOMETRY	11
3.8	COMPARING THE NUMERICAL RESULTS FROM DIFFERENT INSTRUMENTS	12
4	EXPERIMENTAL RESULTS	12
4.1	TOPOGRAPHY AND HOMOGENEITY OF SURFACES	12
4.1.1	Platinum-iridium	12
4.1.2	Pure iridium	15
4.1.3	Gold platinum alloy	18
4.1.4	Ni-based superalloy (U720)	18
4.1.5	Stainless steel	18
4.1.6	Tungsten	21
4.1.7	Silicon	24
4.2	SURFACE CONTAMINATION MEASUREMENTS	24
4.2.1	XPS measurements (NPL)	24
4.2.2	XPS measurements (EJPD)	31
4.2.3	XRF Measurements	34
4.3	SiO ₂ THICKNESS MEASUREMENTS	38
4.4	ROUGHNESS SURFACE CHARACTERISATIONS	39
4.5	COMPARISON OF SURFACE ROUGHNESS BY WHITE LIGHT INTERFEROMETRY ..	41
5	DISCUSSION	43
5.1	SURFACE ROUGHNESS	43
5.2	SURFACE CONTAMINATION	44
6	CONCLUSION	44

1 INTRODUCTION

The report details the outcome of Deliverable 1.1.4 of EMRP Project SIB05 (NewKILO). The aim of this deliverable was to characterise materials and production techniques for the new generation of mass standards to be used in the watt balance experiments and as primary standards to ensure the dissemination and maintenance of the unit of mass with a target uncertainty of about 10 μg .

Within the scope of the watt balance and Avogadro experiments, which aim at linking the unit of mass to a fundamental constant rather than a material artefact, it is necessary to achieve a direct link between the primary realisations and the reference mass standards that ensure the reliable dissemination of the mass scale. To ensure the mid/short term stability (1 to 10 years) of the new definition and to realise its dissemination with the lowest uncertainties, knowledge of the behaviour (in terms of mass stability) of materials from which mass standards are constructed is essential.

The properties of nine materials were examined to assess their suitability for use as mass standards to disseminate the unit of mass from the new primary realisations.

2 MATERIALS USED IN THE STUDY

The materials were evaluated for the properties required when used in the primary realisation experiments and as primary standards for the medium term maintenance and the dissemination of the redefined unit of mass. The density, hardness, magnetic permeability and surface sorption characteristics of the materials (in increasing order of importance) determined which were the most suitable. Selected materials include the platinum-iridium alloy currently used for primary mass standards, pure iridium, gold platinum alloy, stainless steel, (SS), Ni-based superalloy (U720) and single and poly crystal tungsten. With respect to PtIr, tungsten and iridium are comparably dense but harder and have lower magnetic susceptibilities. Stainless steel is the metal from which most secondary kilogram standards are made. Udimet720 has similar density but is much harder and has a lower magnetic susceptibility. However, it cannot replace stainless steel for secondary standards because its density is slightly greater (8800 $\text{kg}\cdot\text{m}^{-3}$ vs 8000 $\text{kg}\cdot\text{m}^{-3}$). The microstructure of the materials was also examined, as this affects properties such as hardness, ease of machining and therefore mass stability.

In addition, two composite materials were manufactured and investigated namely electroplated rhodium and gold layers on bulk copper. The aim here was to combine good bulk properties such as high density and homogeneity and low magnetic susceptibility with favourable surface properties, namely hardness and chemical resistivity. For more detail see the report for deliverable D 1.2.2.

Also investigated was silicon, which has many of the properties required for the watt balance experiment (high hardness, low magnetic susceptibility and low surface sorption coefficient) and is used in the Avogadro project. This material has the advantage that it immediately produces natural oxides, which protect the surface from the surrounding environment. This task studied the growth of oxides by thermal heat treatments in order to evaluate the efficiency of the protective layer. In addition to samples with natural oxide, two heat treatments were performed to produce SiO_2 coatings of thickness 5 nm and 10 nm.

Since it was not practical to distribute the same sample of each material among all laboratories involved in the work package, 9 or 12 samples were produced of each material and distributed to individual laboratories. Shipping documents [1] outline the number of samples of each material provided and identifies them by number.

The properties of the nine materials tested are given in Table 1.

Table 1: Physical properties of the selected materials (*hardness of coating).

Material	Density (kg.m ⁻³)	Hardness (HV)	Magnetic susceptibility ($\chi_v \times 10^{-5}$)	Provider	Number of samples
PtIr	21530	175	+24	BIPM	12
AuPt	15870	250	-2.8	BIPM	12
Ir	22500	380	+5.9	LNE-Cnam	12
W	19300	740	+5.5	NRC	12
Si	2300	1000	-0.3	PTB	9
Stainless steel	8000	200	+300	EJPD	9
U720	8100	500	+44	LNE	9
Cu ep with Au	8937	200 – 230*	-10 (bulk Cu)	EJPD	12
Cu ep with Rh	8937	600 – 900*	-10 (bulk Cu)	EJPD	12

3 TECHNIQUES USED

Different complimentary techniques have been used to characterise the homogeneity and the cleanliness of the selected materials. Atomic Force Microscopy (AFM), Scanning Electron Microscopy (SEM) and coherence scattering interferometry (CSI) were used to evaluate the topography and the surface texture of the samples. The surface chemistry (contamination) was analysed by X-ray Photoelectron Spectroscopy (XPS) and X-ray Fluorescence (XRF), whereas the thickness of silicon oxide layers was determined by Spectral Ellipsometry (SE).

A short description of the different techniques used is given below.

3.1 ATOMIC FORCE MICROSCOPY

Atomic force microscopy (AFM) is a high resolution form of scanning probe microscopy in which the scanning “tip”, attached to a cantilever, interacts with the surface being scanned via inter-atomic forces. This allows a high z -axis sensitivity of typically less than one nanometre. The AFM studies were performed at the Centre for Metrology and Accreditation (MIKES) using a Park XE-100 AFM, operated in non-contact mode. Surface topography maps were recorded with scan sizes of 20 $\mu\text{m} \times 20 \mu\text{m}$ and 5 $\mu\text{m} \times 5 \mu\text{m}$ with a resolution of 256 pixels \times 256 pixels. Based on these images, areal surface texture parameters were calculated. Standard silicon cantilevers (AppNano, type ACTA) with tip radius of < 10 nm were used for the studies.

3.2 SCANNING ELECTRON MICROSCOPY

Scanning Electron Microscopy (SEM) images a sample by scanning it with a focused beam of electrons. The electrons interact with sample and give information about the sample's surface composition. The SEM studies were performed in Finland but at Aalto University, School of Chemical Technology, Department of Materials Science and Engineering using a Hitachi S-4700 cold field emission electron gun instrument equipped with a semi-in-lens detector. High resolution electron micrographs from the surfaces were taken at magnifications of $\times 700$, $\times 20,000$ and $\times 70,000$ utilizing low acceleration voltage (5 kV). No sample coating was applied.

3.3 ANGLE RESOLVED SCATTERING

The optical roughness meter of CNAM performs in-plane measurements using a monochromatic laser source ($\lambda \approx 635 \text{ nm}$), an optical collimation and filtering system, a motion-controlled sample holder, a detector on a movable arm and a photomultiplier tube (see figure 1).

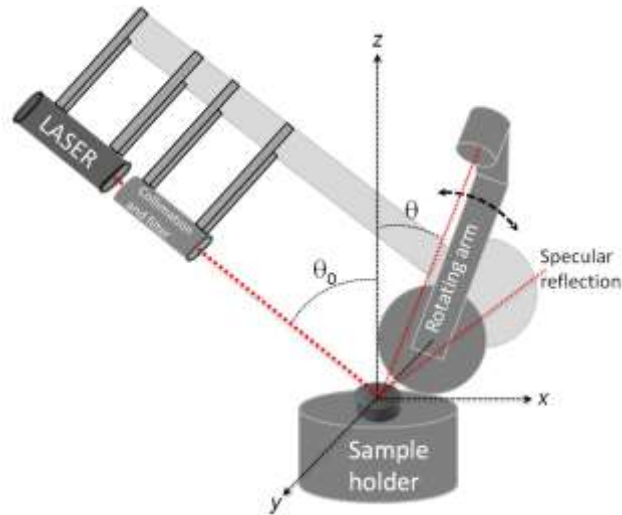


Figure 1. Schematic diagram of the optical roughness meter.

The surface is illuminated (see figure 2) under oblique incidence by p -polarized monochromatic light. Measurements of the angular distribution of the scattered light are taken in the plane of incidence. It takes about 2-3 minutes to measure the angular distribution of the scattered light for a given site on a sample, which makes the method relatively fast compared to others. Angle-resolved scattering (ARS) theory allows the angular distribution of the scattered light to be related to the surface roughness using the Power Spectral Density (PSD). The use of an appropriate analytic model of the PSD allows one to determine the Root Mean Square (*rms*) height of the asperities as well as their transverse correlation length. For detailed explanations see the article by Zerrouki *et al.* [2].

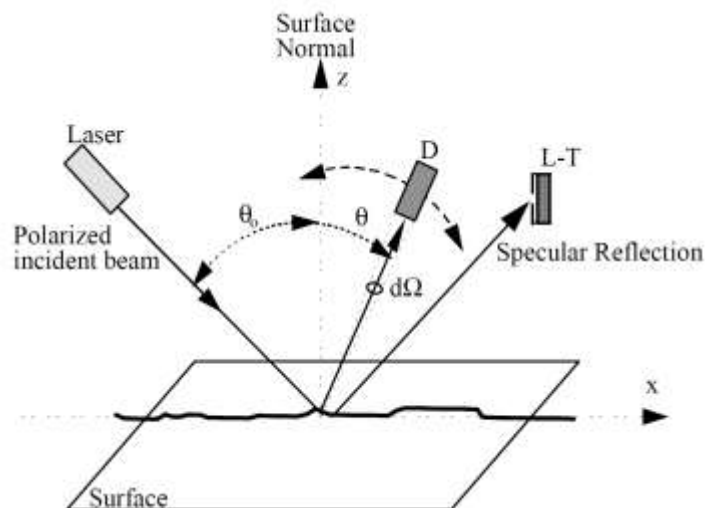


Figure 2 - Experimental set-up
(D: Detector; L-T: Light Trap; $d\Omega$: elementary solid angle).

The number of analysed sites is determined from the size of the sample. For the 10 mm diameter cylindrical samples of Ir, Udimet 720, Au ep Cu and Rh ep Cu, 10 sites were analysed. For square silicon samples (20 MM \times 20 mm), 25 sites are analysed to provide a fair representation of the surface.

3.4 COHERENCE SCATTERING INTERFEROMETRY

The surface roughness of sample materials was also determined using an optical reflection method by measuring the intensities of totally and diffusely reflected white light with an integrating sphere [1, 2]. The roughness scale was calibrated with reference samples of known roughness. Surface roughness studies were performed using the same samples as those studied with SEM.

For the Rh coated Cu samples, roughness measurements at EJPD were performed using a white light microscope (WLM).

3.5 X-RAY PHOTOELECTRON SPECTROSCOPY

X-ray photoelectron spectroscopy (XPS) measures the energy of electrons emitted from a surface by means of a focussed beam of X-rays. It gives quantitative (and stoichiometric) information on the (chemical) composition of the surface under investigation. XPS measurements were carried out at NPL using a Kratos Axis Ultra instrument. Survey spectra in the range 0 eV to 1400 eV binding energy were taken at emission angles of 0° and 60° to the surface normal from an area of each sample using an Al monochromated X-ray source operated at 15 kV, 5 mA emission. Analysis conditions used were 160 eV pass energy, 1 eV steps, 0.2 s dwell per step and a single scan. The survey scans were corrected using the latest NPL transmission function calibration and Average Matrix Relative Sensitivity Factors (AMRSFs) were applied.

At NPL X-ray photoelectron spectroscopy (XPS) was carried out using a Kratos Axis Ultra. Survey spectra in the range 1400 eV to -10 eV binding energy were taken at emission angles of 0° and 60° to the surface normal from an area of each sample using an Al monochromated X-ray source operated at 15kV, 5mA emission. Analysis conditions used were 160 eV pass energy, 1 eV steps, 0.2 sec dwell per step and 1 scan. The survey scans have been corrected using the latest NPL transmission function calibration and Average Matrix Relative Sensitivity Factors (AMRSFs) were applied.

At EJPD the cleanliness and the chemical composition of the samples was analysed using an alpha110 XPS system. For enhanced surface sensitivity, all spectra were taken at an emission angle of 60°. Survey spectra (pass energy 50 eV, step 1 eV) using a Mg X-ray source at 300 W were combined with narrow scans (pass energy 20 eV, step 0.2 eV) for quantitative analysis.

3.6 X-RAY FLUORESCENCE

X-ray Fluorescence (XRF) examines the absorption of radiation (from an X-ray source) and the re-emission of radiation of a different energy to characterise the (chemical) composition of a surface. X-ray spectrometric measurements were performed at PTB's laboratory at the synchrotron radiation facility BESSY II using the plane grating monochromator (PGM) and the four crystal monochromator (FCM) beamline. The light elements (B to Al) have been measured at the PGM beamline and the K-fluorescence emission was observed. All the heavier elements have been measured at the FCM beamline. For the mid-range elements (Si - Zn) the K-lines were observed, but in the case of the heavy matrix components only the L-lines (W) and the M-lines (W, Ir, Au) were observable. Using M-lines for a quantitative analysis is very problematic, because of the bad quality of the tabulated data for M cross sections. This is one reason why we have provided only estimates for the bulk contamination.

The XRF measurements were performed in an UHV chamber ensuring conventional 45°/45° beam geometry. A sketch of the set-up is shown in figure 3. For the excitation of the samples, monochromated synchrotron radiation has been used. The measurements in the soft X-ray range (<1.8 keV) have been performed at PTB's plane grating monochromator (PGM) beamline for undulator radiation and the measurements in the hard X-ray range have been carried out at the four crystal monochromator (FCM) beamline for dipole radiation.

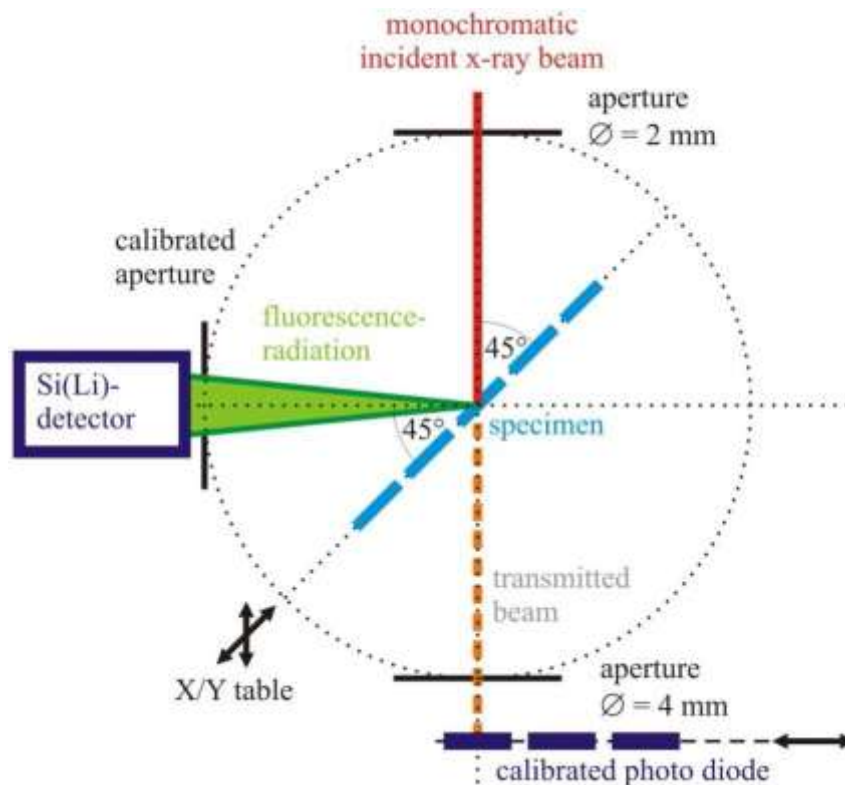


Figure 3: Experimental set-up used for the XRF measurements in conventional 45°/45° beam geometry. The employed energy-dispersive detector was a radiometrically calibrated Silicon Drift Detector (SDD).

3.7 SPECTRAL ELLIPSOMETRY

Ellipsometry is an optical measurement technique used to characterise the thickness (or optical constants) of thin films (tens of micrometres). The method involves measuring the polarization change of light reflected from surface under investigation..

Two 6'' (152.4 mm) diameter wafers with a SiO₂ coating, with thicknesses of about 5 nm and 10 nm, were measured with spectral ellipsometry. Two objectives were addressed with these measurements:

1. Determination of the SiO₂ film thickness.
2. Variation of the thickness over the surface area.

For calibrated measurement of SiO₂ thicknesses at PTB, a spectral ellipsometer from Semilab (formerly Sopra) type GES-5E was used. In this measurement the instrument is used as a comparator, *i.e.* before and after the measurement of the samples, the reference set 2 of PTB, with certified thickness values are measured. The traceability of these reference set is realized through X-ray reflectometry (XRR) determination of the SiO₂ thickness. The thickness values (dSiO₂) for the samples are calculated from the ellipsometric thicknesses (dSiO₂, SE), which are obtained from the raw data via fitting.

The sample discs were divided into 32 sectors (See figures 39 and 40). The sample holder of the ellipsometer used for these measurements is equipped with an linear translation stage which allows a range of movement of the samples of 200 mm (*x*-direction) and a second perpendicular translation stage (*y*-direction) with 40 mm displacement. Therefore it was possible to perform defined positioning of the

sample over a complete row (x -direction) and a movement for three rows (y -direction) (See figures 39 and 40). Consequently, a manual repositioning of the sample in the sample holder was required to cover the complete area of the wafer.

For the determination of the thickness variation in the centre of each chip ($20\text{ mm} \times 20\text{ mm}$) an ellipsometry measurement was carried out, using the CCD sensor of the ellipsometer. The positioning uncertainty is estimated to be roughly $\pm 5\text{ mm}$ for both the x - and z -directions.

3.8 COMPARING THE NUMERICAL RESULTS FROM DIFFERENT INSTRUMENTS

It should be noted that using the concept of roughness δ is not sufficient for characterizing the surfaces; two surfaces could have the same value of δ with different topographies. In this case it is useful to consider the Power Spectral Density (PSD) which give information on asperity contribution for different spectral domains. An additional useful piece of information which is provided by optical roughness meters such as AFM and STM is the PSD which often a good indication of the signature of the surface under study.

Usually, mechanical technicians will describe surface roughness in parametric terms of a single numerical value such as R_a , R_z , or R_q . This is why one extracts from PDS the RMS height which is only a qualitative figure of merit of the surface quality. It is not traceable dimensionally and it depends on the spatial frequency band used (a function of laser wavelength, angles of incidence and detection).

There is no single roughness value one can attribute to a surface because each method used covers different spectral ranges of surface spatial wavelength. Consequently, each one gives a different value of RMS roughness (R_q). The main difficulty lies in the interpretation and comparison of the results obtained from different instruments. It is thus necessary to have further information at one's disposal together with values of the surface parameters provided by a roughness measurement technique. For instance, the RMS heights (R_q) obtained from AFM topographic ($20\text{ }\mu\text{m} \times 20\text{ }\mu\text{m}$) and ($5\text{ }\mu\text{m} \times 5\text{ }\mu\text{m}$) scans are often different because the analysis windows (*i.e.* the spatial frequency ranges) are different. Additionally the filters which are applied to the raw measurement data will have a significant effect on the surface roughness calculated.

4 EXPERIMENTAL RESULTS

4.1 TOPOGRAPHY AND HOMOGENEITY OF SURFACES

4.1.1 Platinum-iridium

The platinum-iridium sample scans at different levels of magnification are shown in figures 4 – 6. Parallel grooves resulting from polishing the samples during manufacturing can be clearly seen on the surface. A small amount of surface contamination was found near the scratches of the surface.

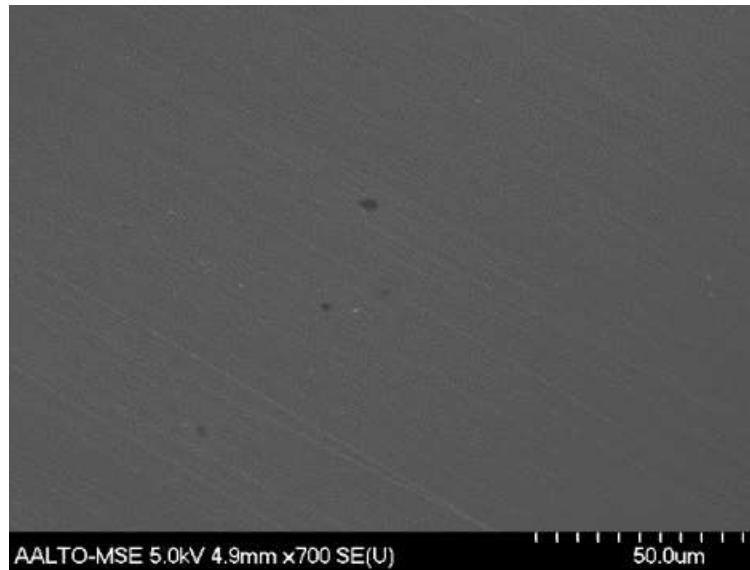


Figure 4. SEM micrograph at $\times 700$ magnification of platinum-iridium sample surface.



Figure 5. SEM micrograph at $\times 20,000$ magnification of platinum-iridium sample surface.

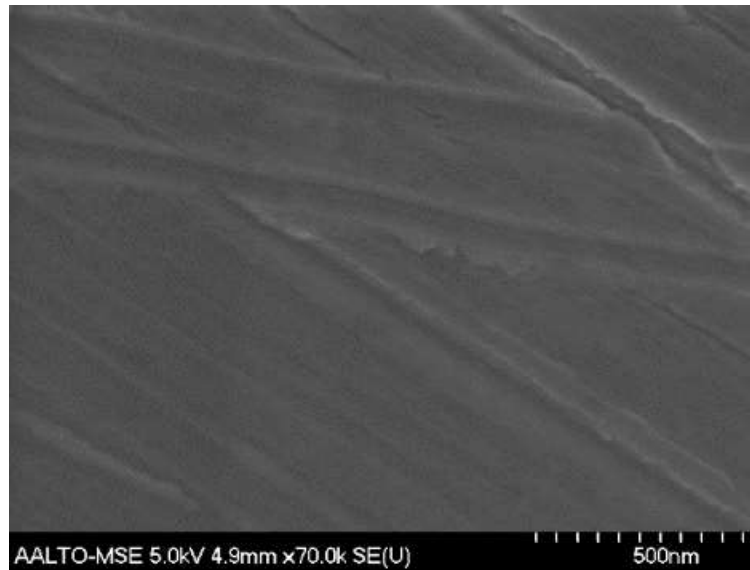


Figure 6. SEM micrograph at $\times 70,000$ magnification of platinum-iridium sample surface.

The AFM images of the platinum-iridium surface (figures 7 and 8) resemble the SEM images in that the surface appears rather smooth and that there are parallel scratches. However, more contamination (seen as light areas in the images) was found on the sample studied with the AFM. The AFM studies were conducted using different samples and thus differences in sample cleanliness might explain this. However, loosely attached contamination might have come off in the ultra-high vacuum of the SEM, resulting in a cleaner surface than measured with AFM (in air).

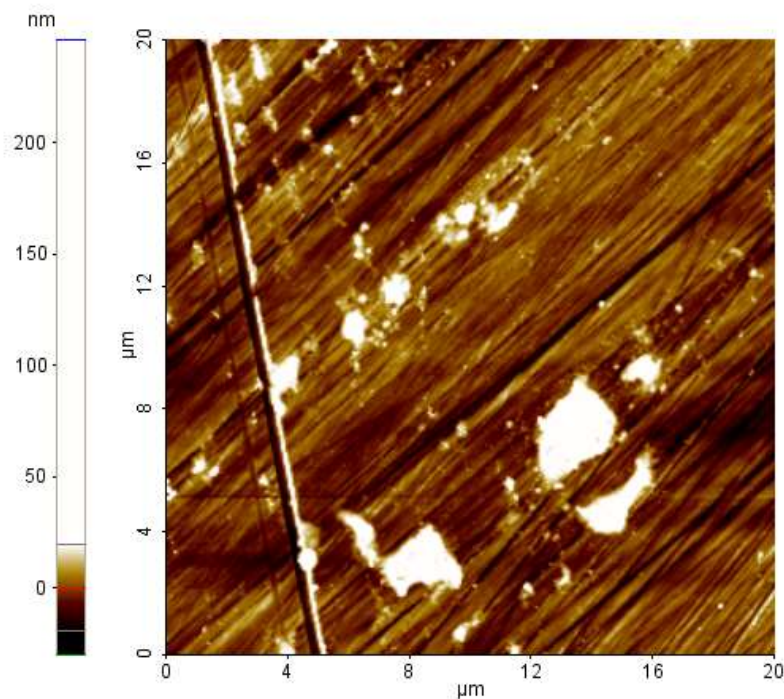


Figure 7. AFM topography image of platinum-iridium surface taken with a scan size of $20\ \mu\text{m} \times 20\ \mu\text{m}$.

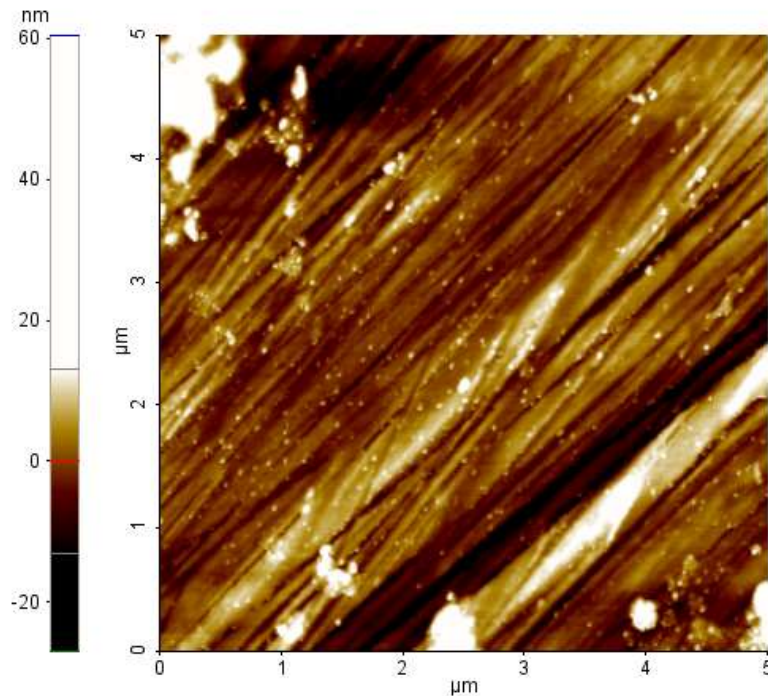


Figure 8. AFM topography image of platinum-iridium surface taken with a scan size of 5 μm \times 5 μm .

4.1.2 Pure iridium

Sample preparation

The preparation of the iridium sample surface by the CNAM was different from that used for PtIr samples at BIPM, owing to the greater hardness of Ir compared with the PtIr alloy.

The CNAM polishing process applied for iridium and Ni-based superalloy (Udimet720) samples was a mechanical one that uses abrasive particles in successively finer steps to remove material from the surface, until the required result is reached. The first step is the grinding process involving SiC-Paper to remove damaged or deformed surface material. The goal is to produce a plane surface with minimal damage that can be removed easily during polishing in the shortest possible time. The final step is diamond polishing. Diamond is used for hard materials as an abrasive to accomplish the fastest material removal and the best possible planeness. Diamond polishing is carried out on polishing cloths and a lubricant must be used. Diamond grains sizes from 9 μm to 0.25 μm are used. Each grain of different granularity has its own support (polishing cloth) in order to be free of any contamination by the previous grains from the preceding step of polishing.

Samples are polished with the Struers polishing machine TegraPol 35 for 300 mm discs, equipped with the specimen mover Tegraforce 5. Up to 6 single specimens can be inserted in the specimen mover plate, where the force is applied individually to each specimen. The polishing system is equipped with a variable disc speed of 40-600 rpm and variable specimen mover head speed of 50-150 rpm. Reproducibility is ensured by automated process control by choosing the appropriate speeds of the polishing disc and mover plate, their direction of rotation and the force applied on the samples and the duration of each polishing step.

The protocol requires that samples be cleaned between each preparation step. The cleaning process is performed using an unheated ultrasonic bath (Struers Metason 200 HT) filled with 95% ethanol.

Results

The iridium sample scans are shown in figures 9 to 11. Smaller and fewer grooves were found on iridium than on platinum-iridium and the scratches were randomly orientated. This is because the polishing process used for the iridium surface was different from that applied to the platinum-iridium surface at the BIPM.

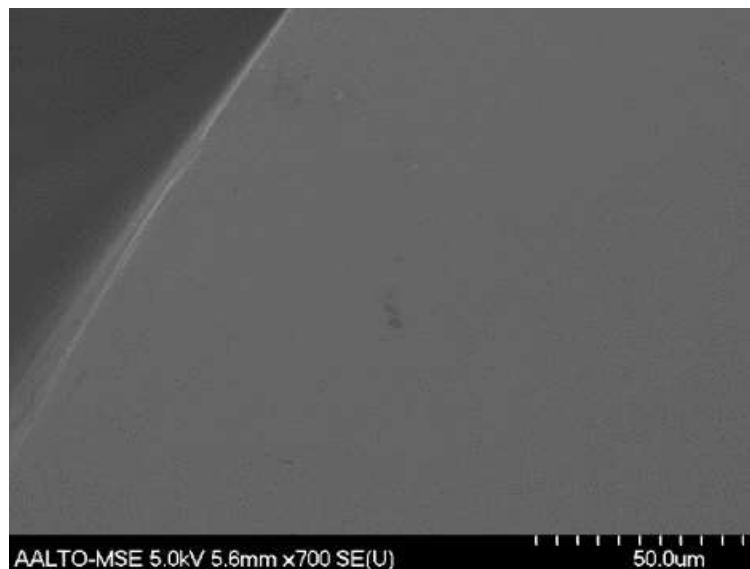


Figure 9. SEM micrograph at $\times 700$ magnification of iridium sample surface.

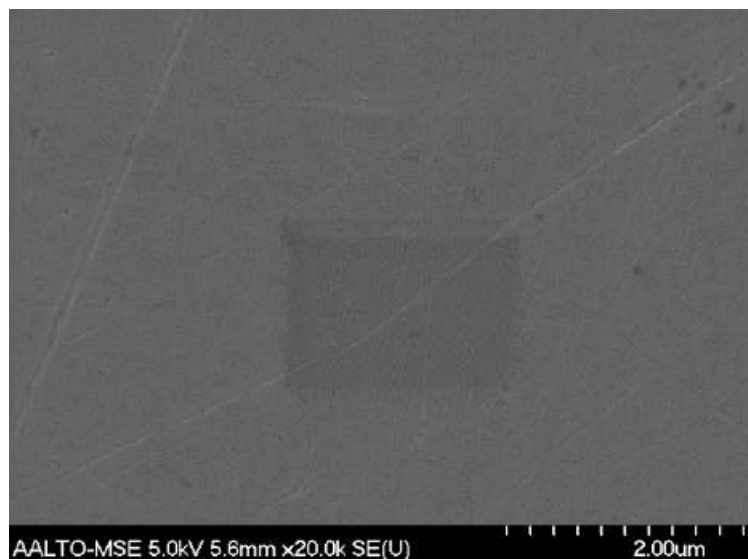


Figure 10. SEM micrograph at $\times 20,000$ magnification of iridium sample surface.

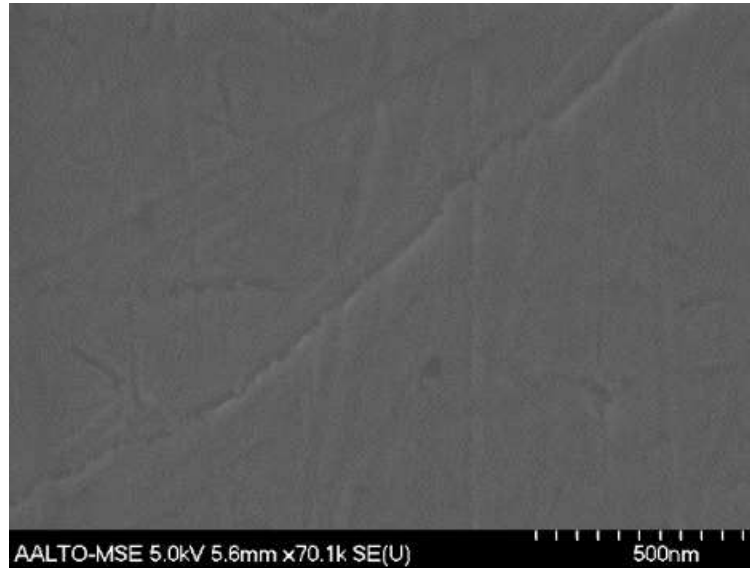


Figure 11. SEM micrograph at $\times 70,000$ magnification of iridium sample surface.

The AFM images of the iridium surface are shown in figures 12 and 13. Randomly oriented scratches, which are smaller than those observed on the platinum-iridium, are also seen in the AFM figures. Again the AFM images show surface contamination not seen in the SEM images. The amount of surface contamination is, however, much less than seen on platinum-iridium. Both the SEM and AFM images show clearly that the iridium samples are cleaner and more homogenous than the platinum-iridium samples.

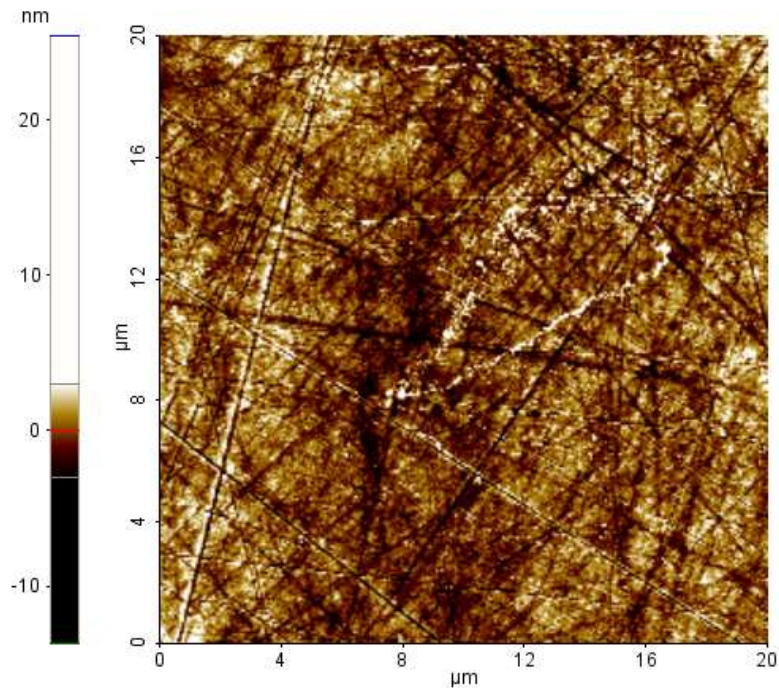


Figure 12. AFM topography image of iridium surface taken with a scan size of $20\ \mu\text{m} \times 20\ \mu\text{m}$.

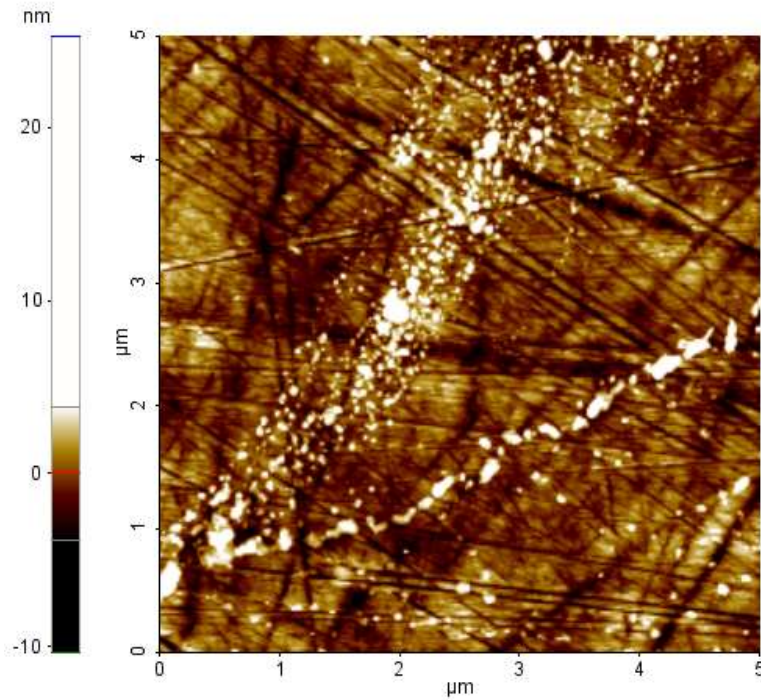


Figure 13. AFM topography image of iridium surface taken with a scan size of 5 μm \times 5 μm .

4.1.3 Gold platinum alloy

See section 4.5.

4.1.4 Ni-based superalloy (U720)

See section 4.4.

4.1.5 Stainless steel

Figures 14 – 16 show SEM images of the stainless steel samples. Visually the samples showed considerably more surface contamination than the platinum-iridium and iridium samples. Also some micro-cracks and pits can be seen on the surface at high magnifications (figure 16). Besides of this, the surface was found very smooth and homogenous. The stainless steel sample had very small grooves, similar to that seen on the iridium sample, indicating that the surface polishing process was very effective.

Additional evidence of the difference between the surface states of the stainless steel, platinum-iridium and pure iridium surfaces can be seen by the oxygen and carbon peaks (figure 17) measured by XPS at EJPD before the samples were characterised by AFM and SEM.

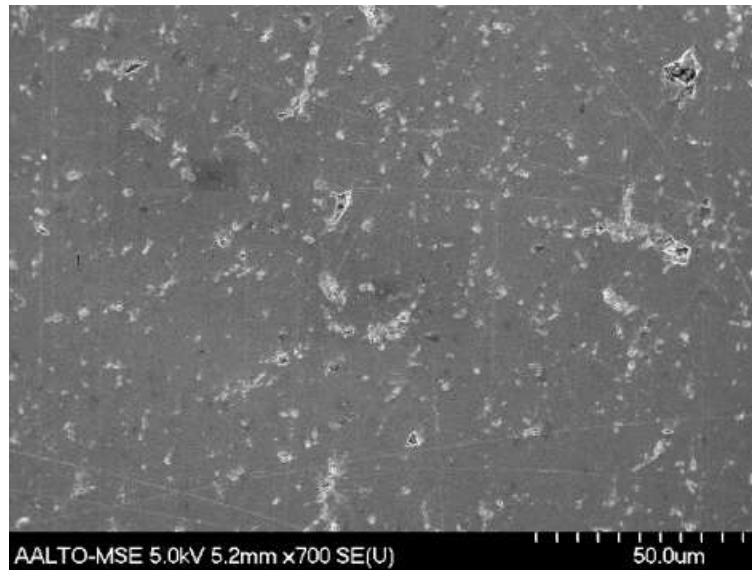


Figure 14. SEM micrograph at $\times 700$ magnification of stainless steel sample surface.

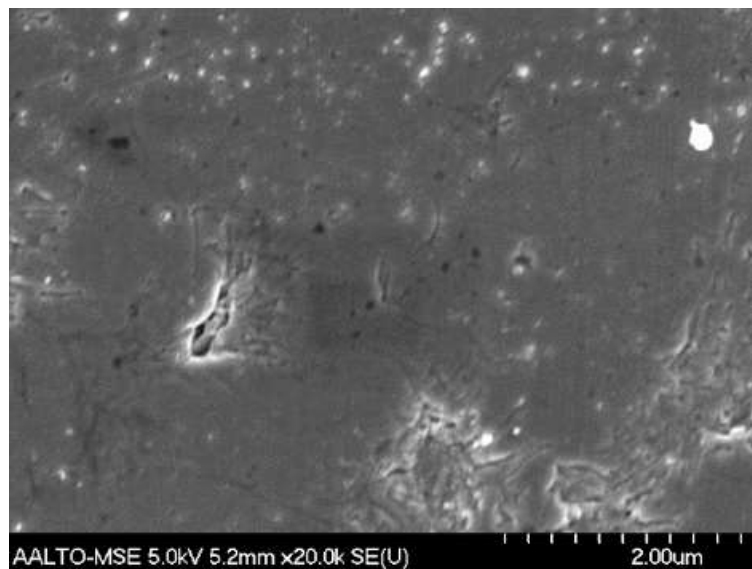


Figure 15. SEM micrograph at $\times 20,000$ magnification of stainless steel sample surface.

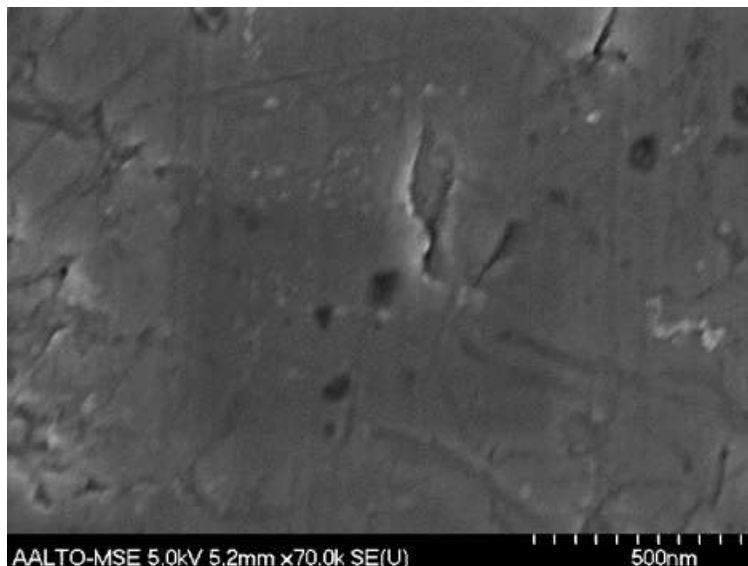


Figure 16. SEM micrograph at $\times 70,000$ magnification of stainless steel sample surface.

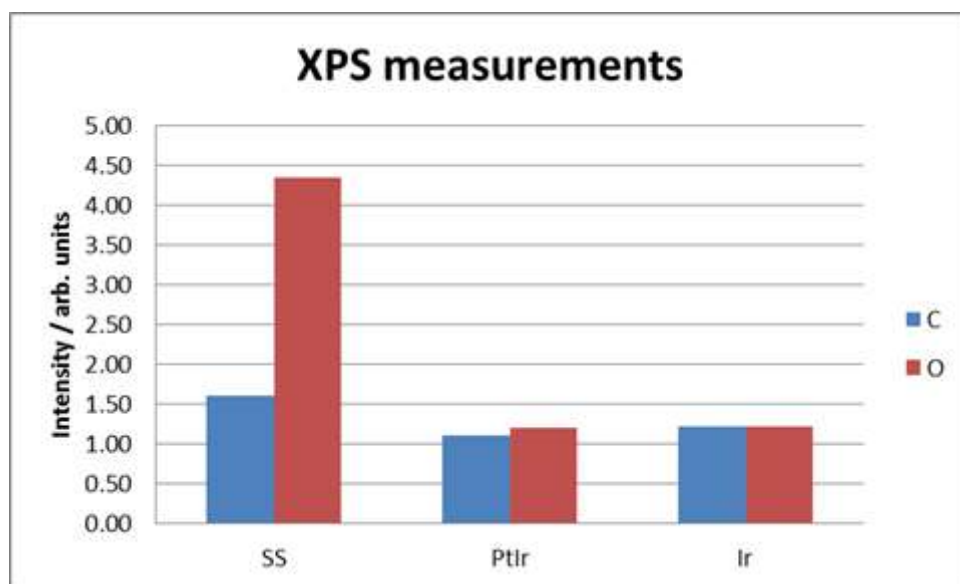


Figure 17. Carbon and oxygen overlayers on stainless steel, platinum-iridium and pure iridium samples measured by XPS at EJPD.

The stainless steel sample analysed with AFM (figures 18 and 19) appears different compared with the one analysed with SEM. The surface had clearly visible randomly oriented grooves, which is typical for polished surfaces. This may indicate that the stainless steel sample was polished and cleaned in a different way than that analysed by SEM. However, the different appearance of the SEM and AFM with respect to grooves might be explained by the different sensitivity of the techniques. Similarly, the AFM images of the tungsten sample identified grooves that were not visible in the SEM images. Despite the different appearance of the stainless steel surfaces, both samples had a very smooth and homogeneous surface.

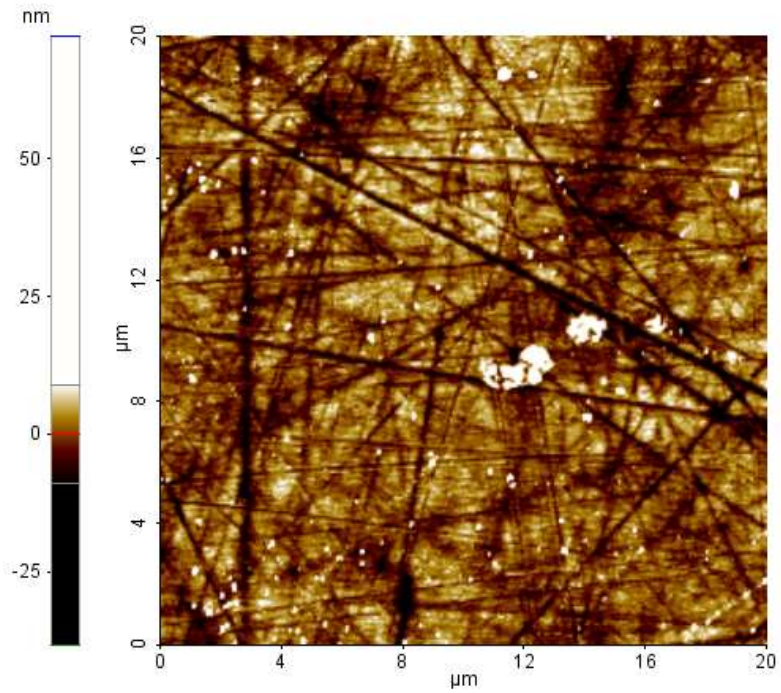


Figure 18. AFM topography image of stainless steel surface taken with a scan size of $20\ \mu\text{m} \times 20\ \mu\text{m}$.

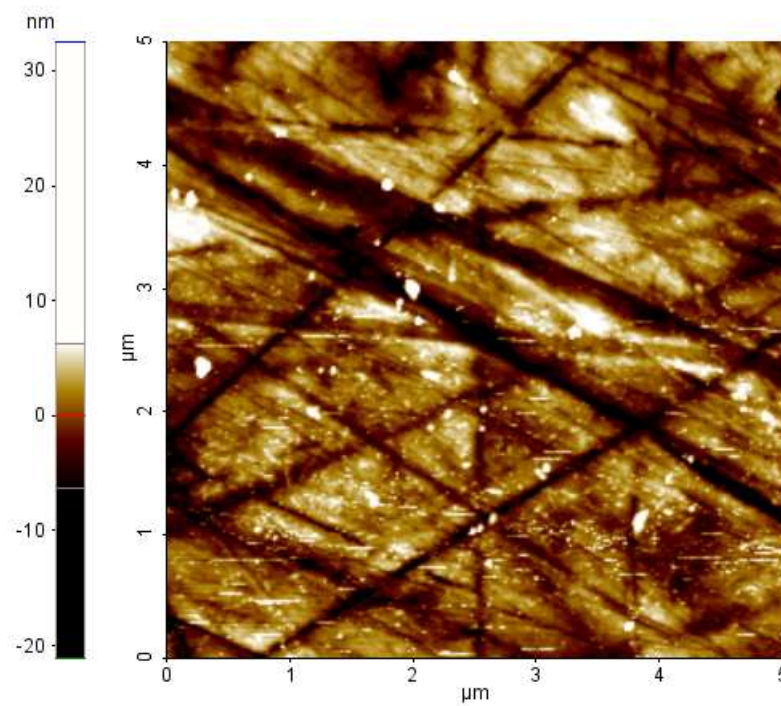


Figure 19. AFM topography image of stainless steel surface taken with a scan size of $5\ \mu\text{m} \times 5\ \mu\text{m}$.

4.1.6 Tungsten

The tungsten surface sample that was analysed with SEM was found to be very smooth and homogenous (figures 20 – 22). No grooves or pits were found.

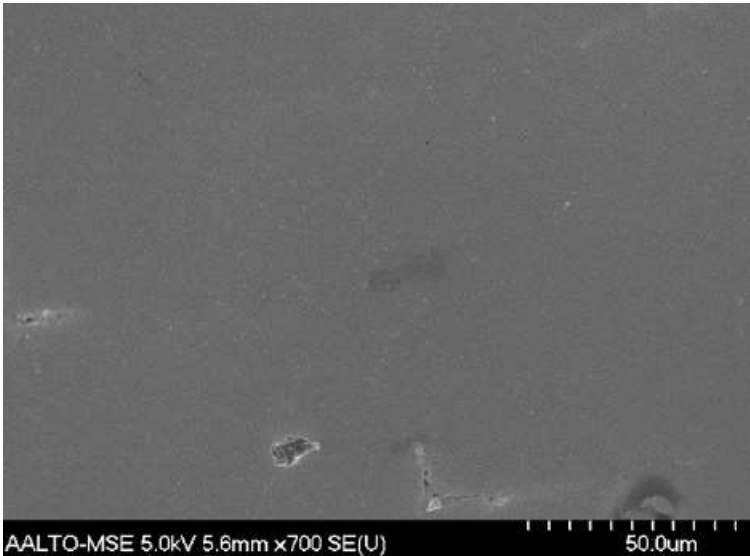


Figure 20. SEM micrograph at $\times 700$ magnification of tungsten sample surface.

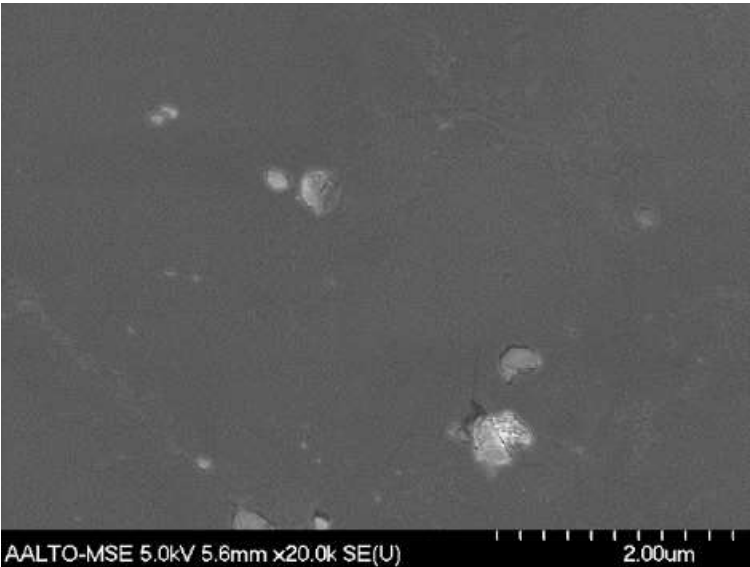


Figure 21 SEM micrograph at $\times 20,000$ magnification of tungsten sample surface.

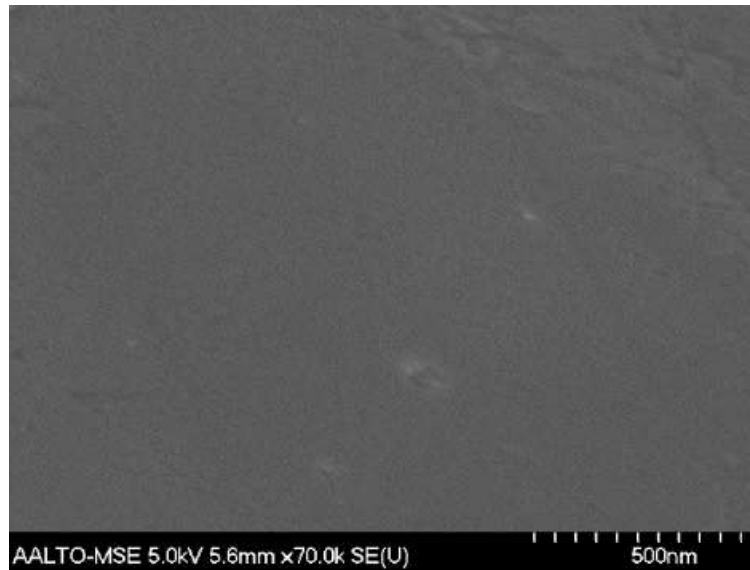


Figure 22. SEM micrograph at $\times 70,000$ magnification of tungsten sample surface.

Again, the surface sample analysed with AFM (figures 23 and 24) look different from the SEM analysed sample. There were grooves and pits not seen on the sample analysed with SEM. Both the SEM and AFM images show, however, that the tungsten surface is very smooth and homogenous with very little surface contamination.

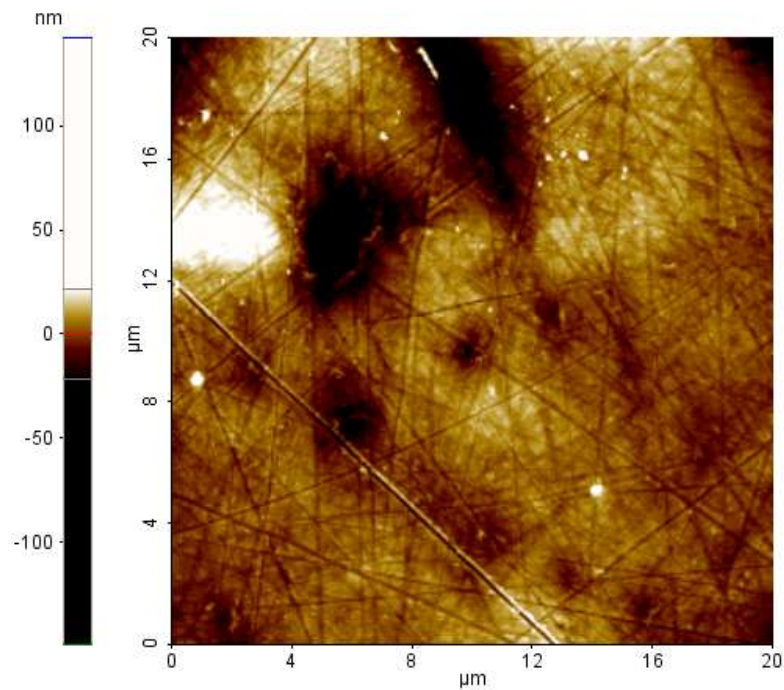


Figure 23. AFM topography image of tungsten surface taken with a scan size of $20\ \mu\text{m} \times 20\ \mu\text{m}$.

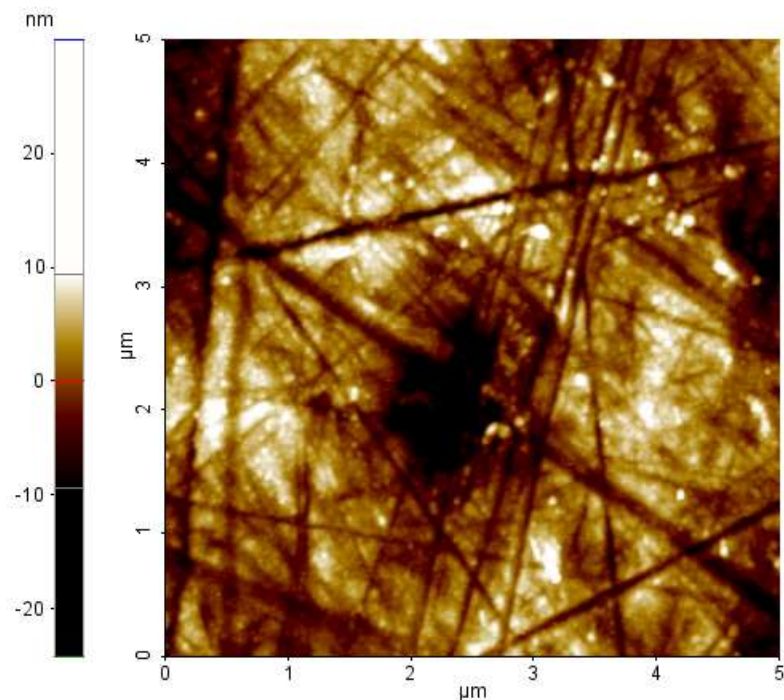


Figure 24. AFM topography image of tungsten surface taken with a scan size of $5\ \mu\text{m} \times 5\ \mu\text{m}$.

4.1.7 Silicon

See section 4.4

4.2 SURFACE CONTAMINATION MEASUREMENTS

4.2.1 XPS measurements (NPL)

The elements identified from the XPS survey spectra acquired at NPL and their atomic percentages measured at an angle of 0° to the surface normal are listed in Table 2 to Table 6, for the Ni-alloy, tungsten, Pt-Ir, iridium and silicon samples respectively. The ratio between the atomic percentage measured at 0° to the surface normal and at an angle of 60° is also given. This additional data may be used to estimate the relative depths of the elements identified, the larger the ratio ($60^\circ/0^\circ$) the nearer the surface the element identified. Example survey scans are shown in figure 25 to figure 29, for the Ni-alloy, tungsten, Pt-Ir, iridium and silicon samples respectively.

The scans of all samples show trace percentages of additional, mainly metallic elements, in particular copper is present in the bulk (rather than on the surface) of all the materials. As expected all materials showed significant carbonaceous and oxide layers on the surface of the samples, with the carbonaceous contamination lying above the oxide layer. With the exception of the silicon all the samples also showed significant traces of nitrogen.

Table 2: Atomic % of the elements identified in the survey scan of the Ni-alloy samples.

Element/shell	Orbital	Atomic % (0° to surface normal)	Atomic % (60° to surface normal)	% Ratio 60°/0°
C	1s	36.8	53.4	1.45
N	1s	1.9	1.4	0.74
O	1s	27.7	25.5	0.92
Ca	2p	0.9	1.1	1.22
Ni	2p	16.4	8.6	0.52
Cu	2p	0.3	0.2	0.67
Co	2p	8.8	5.1	0.58
Mo	3d	0.8	0.5	0.63
Cr	2p	4.5	2.7	0.60
Ti	2p	1.3	0.8	0.62
Cl	2p	0.8	1	1.25

Table 3: Atomic % of the elements identified in the survey scan of the tungsten samples.

Element/shell	Orbital	Atomic % (0° to surface normal)	Atomic % (60° to surface normal)	% Ratio 60°/0°
C	1s	42.6	59.5	1.40
N	1s	1.5	0.7	0.47
O	1s	35.4	26.9	0.76
Cu	2p	4.5	3.2	0.71
W	4d	15.9	9.6	0.60

Table 4: Atomic % of the elements identified in the survey scan of the Pt-Ir samples.

Element/shell	Orbital	Atomic % (0° to surface normal)	Atomic % (60° to surface normal)	% Ratio 60°/0°
C	1s	39.5	55.1	1.39
N	1s	2	0.7	0.35
O	1s	13	13.5	1.04
Cu	2p	2.6	1.7	0.65
Zn	2p	2.2	1.8	0.82
Pt	4f	38	25.4	0.67
Ir	4f	2.7	1.8	0.67

Table 5: Atomic % of the elements identified in the survey scan of the iridium samples.

Element/shell	Orbital	Atomic % (0° to surface normal)	Atomic % (60° to surface normal)	% Ratio 60°/0°
C	1s	36.5	50.4	1.38
N	1s	1.9	2	1.05
O	1s	10.4	12.1	1.16
Cu	2p	2.8	2	0.71
Ir	4f	48.3	33.3	0.69

Table 6: Atomic % of the elements identified in the survey scan of the silicon samples.

Element/shell	Orbital	Atomic % (0° to surface normal)	Atomic % (60° to surface normal)	% Ratio 60°/0°
C	1s	19.7	29.5	1.50
O	1s	31.1	32.7	1.05
Cu	2p	0.42	0.52	1.24
Si	2p	48.7	37.2	0.76
Na	1s	0.1	0.1	1.00

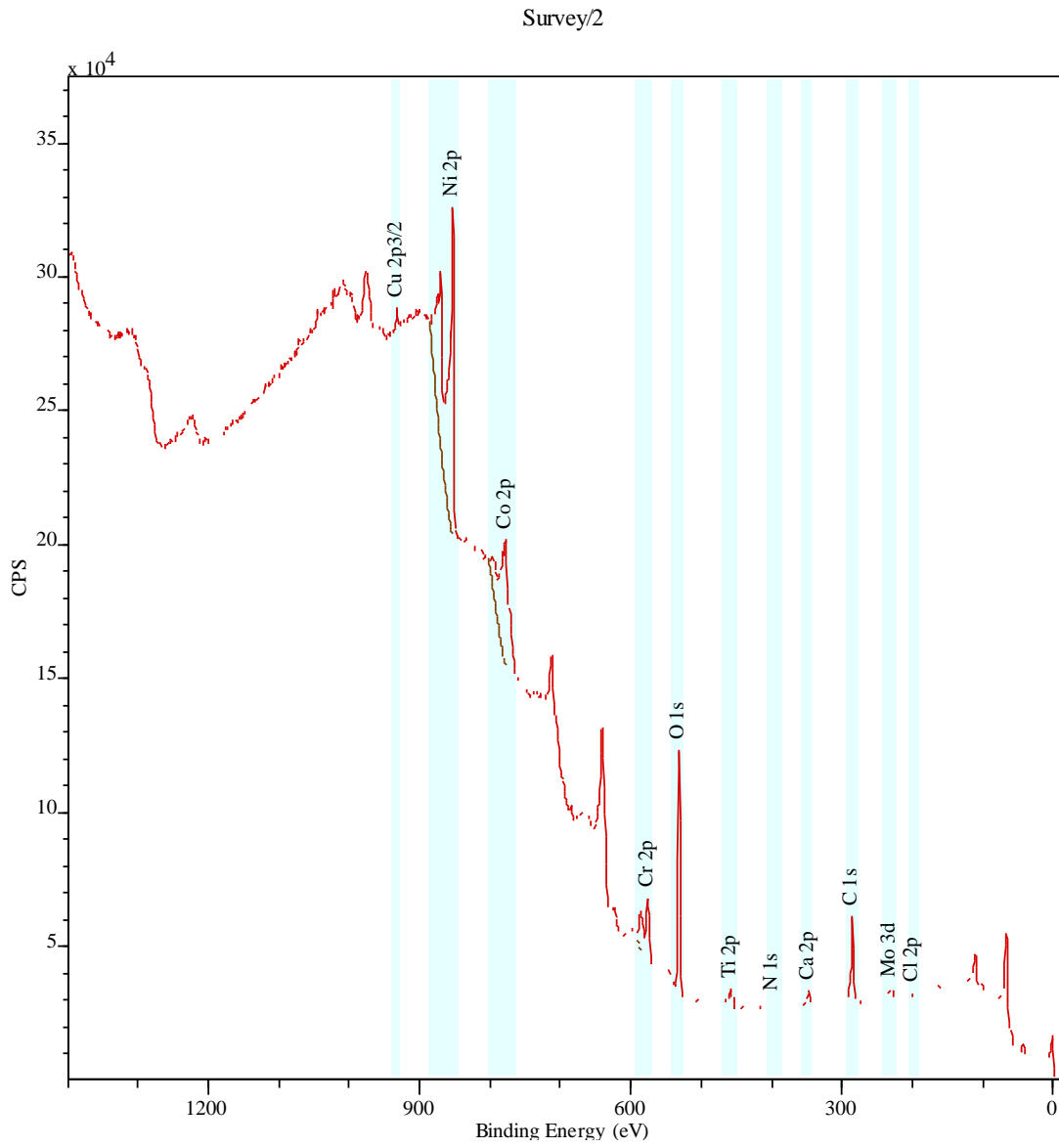


Figure 25: XPS spectrum of (U720) Ni-alloy sample.

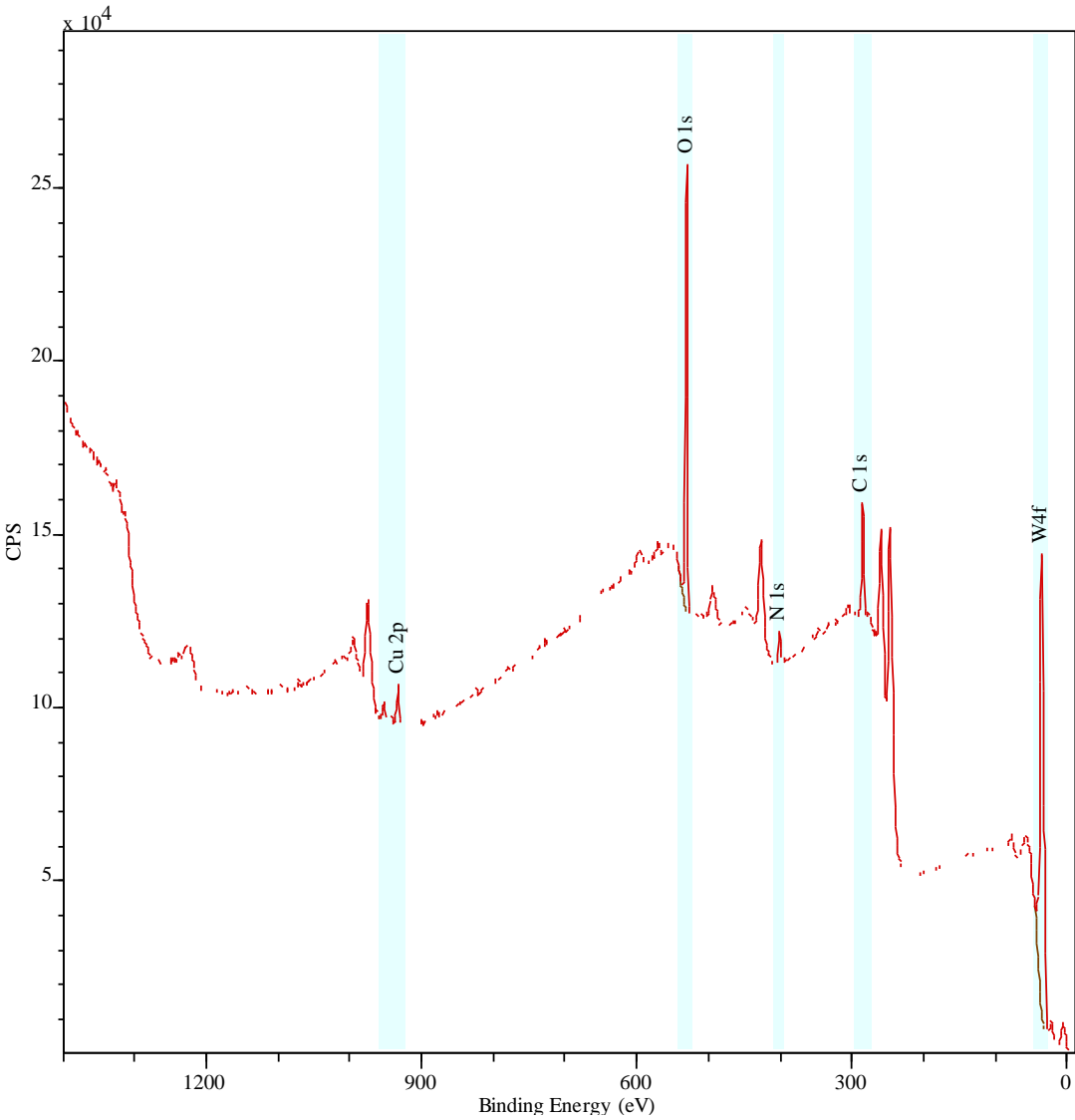


Figure 26: XPS spectra of tungsten sample.

Survey/38

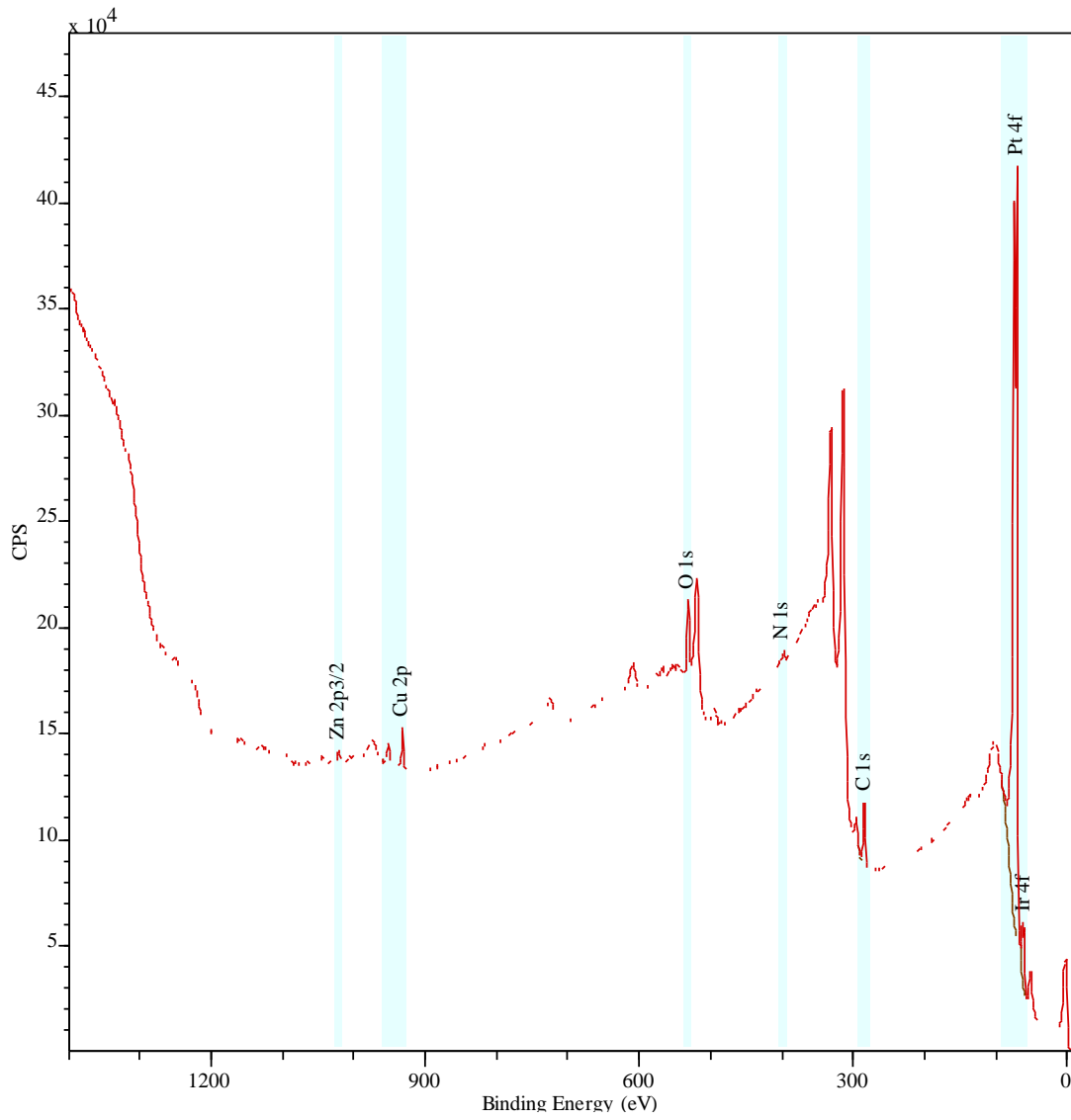


Figure 27: XPS spectrum of Pt-Ir sample.

Survey/56

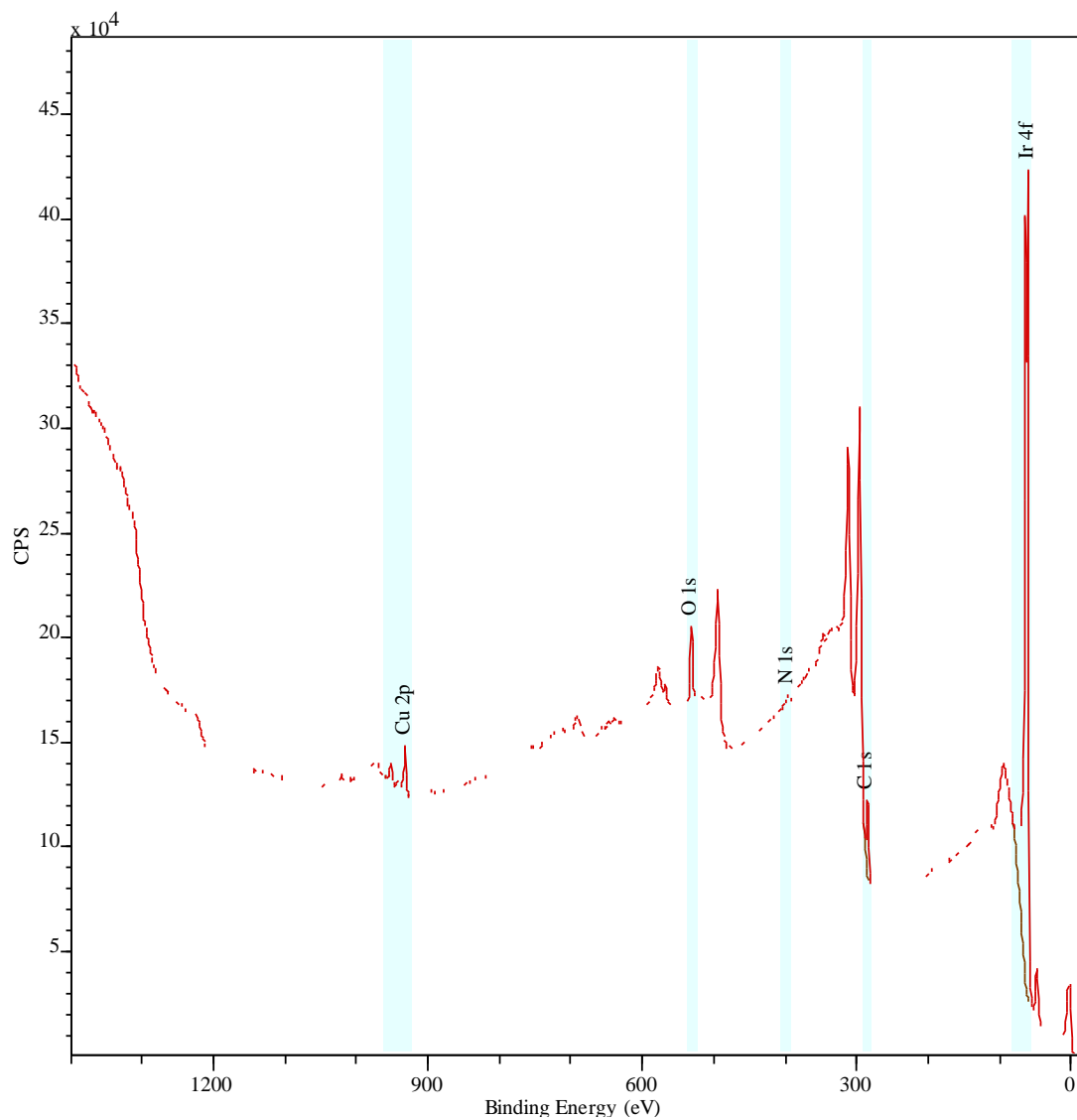


Figure 28: XPS spectrum iridium sample.

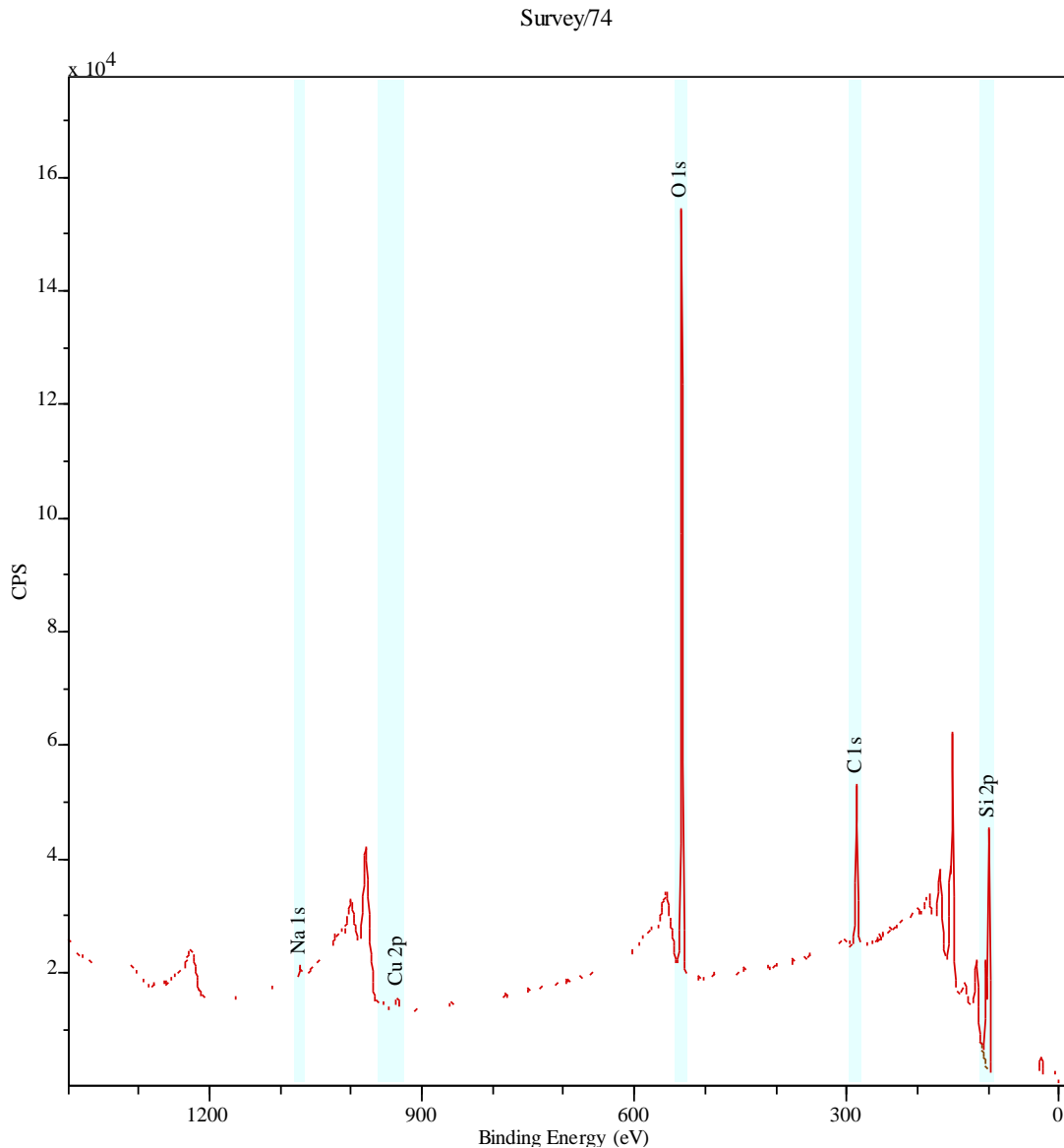


Figure 29: XPS spectrum of Si sample.

4.2.2 XPS measurements (EJPD)

At EJPD the cleanliness and the chemical composition of the samples was analysed using an alpha110 XPS system. For enhanced surface sensitivity all spectra were taken at an emission angle of 60° . Survey spectra (pass energy 50 eV, step 1 eV) using a Mg X-ray source at 300 W were combined with narrow scans (pass energy 20 eV, step 0.2 eV) for quantitative analysis.

The overview XPS spectra of six different materials are shown in figures 30 to 35. The surface chemical composition of the individual materials exhibits a very good homogeneity. Overall the results are very similar to those measured at NPL. The noble metals and alloys are very clean and show contamination by hydrocarbon and oxygen compounds of less than one monolayer. As one might expect, the surface of tungsten has oxidized; we estimate the oxide thickness to be about two to four layers.

All bulk materials show traces of other metallic elements, mainly copper. The origin of these copper traces is not clear. A potential source of contamination is the wet polishing process when copper or

copper alloys are in contact with the polishing liquid. Tungsten is contaminated with 3% copper, a relatively high percentage compared with the other samples where the level is less than 1%.

The electroplated gold and rhodium samples are cleanest and free of copper contaminants. The individual surface chemical composition is described below in the overview scans.

6W / Tungsten

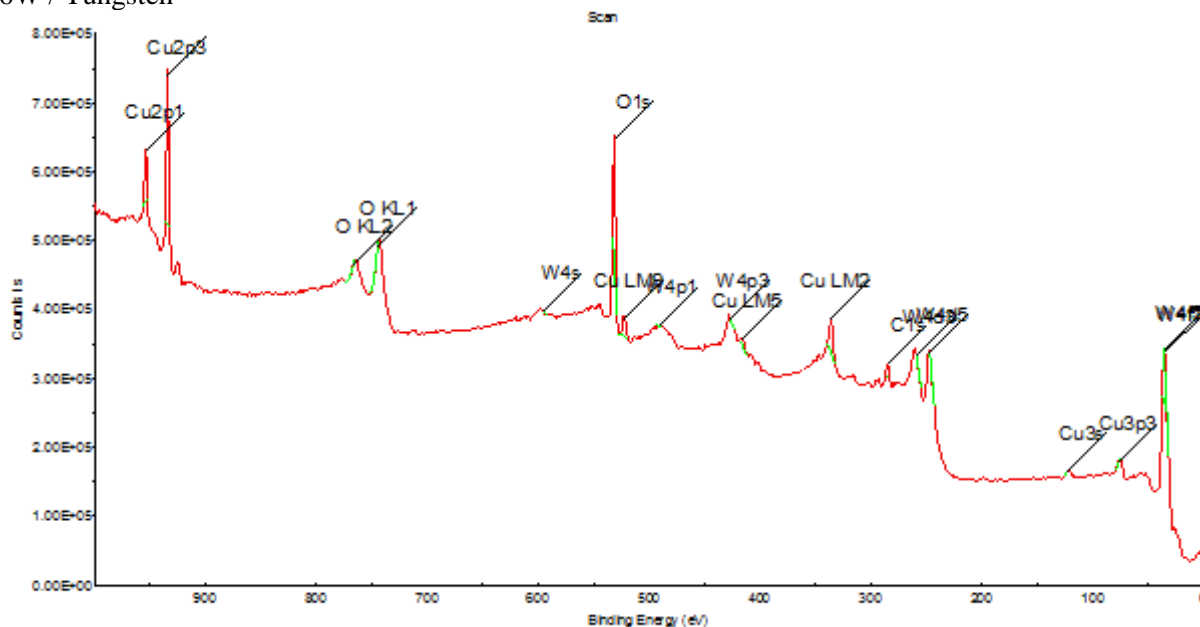


Figure 30: XPS spectrum of tungsten sample. Tungsten exhibits a relatively high contamination of copper; additionally the surface is oxidized.

6Rh / Rhodium

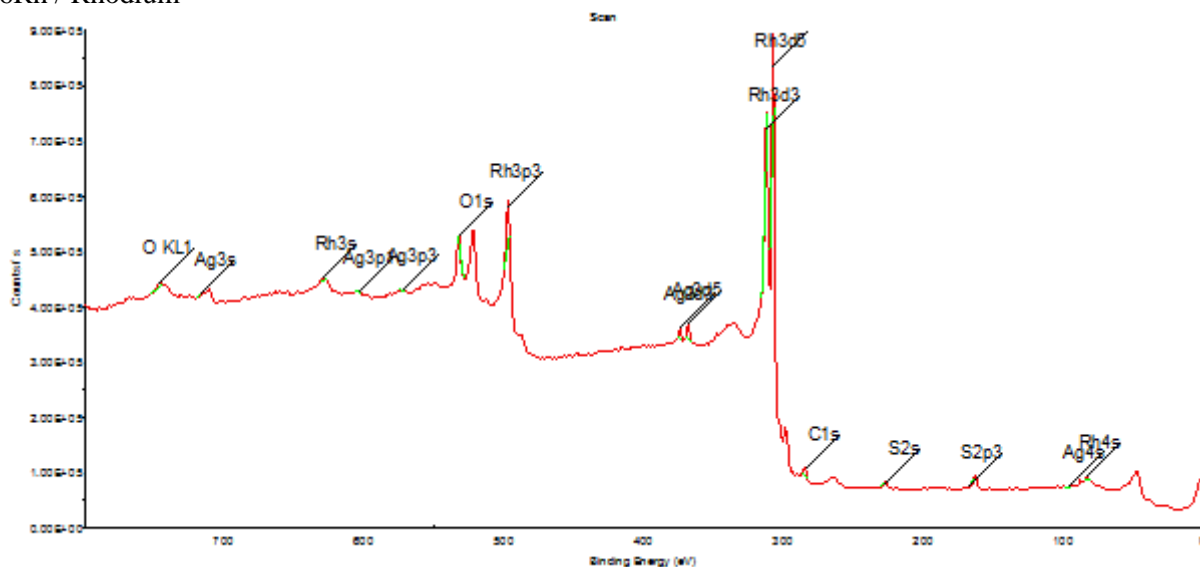


Figure 31: XPS spectrum of rhodium electroplated copper. The rhodium plated surface is also oxidized and exhibits traces of silver and sulphur, but is free of copper.

6Au / Gold

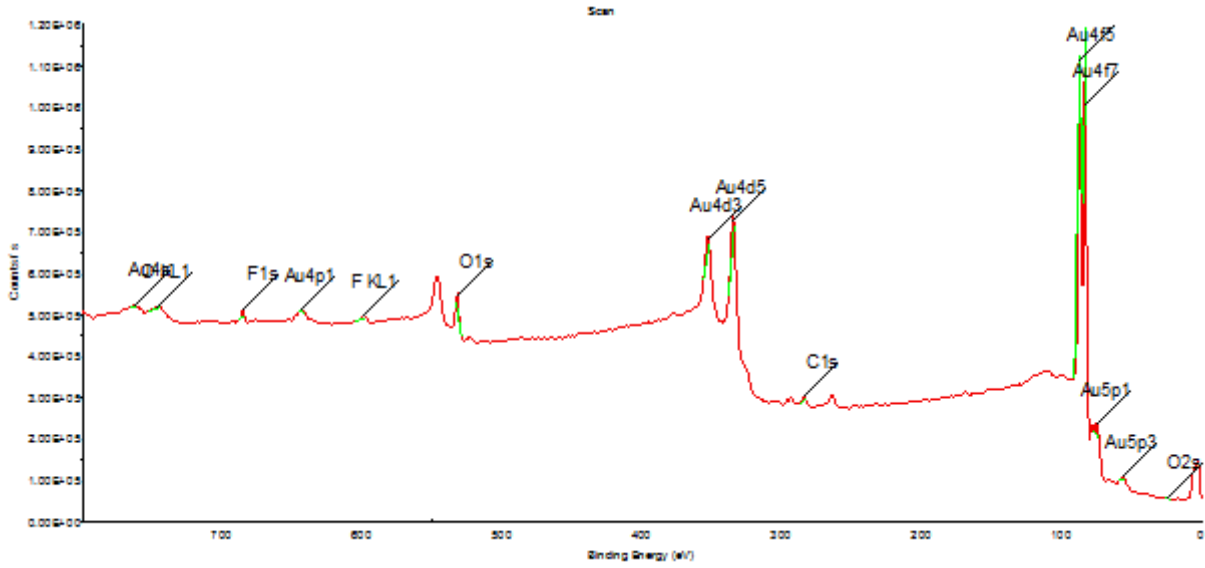


Figure 32: XPS spectrum of gold electroplated copper sample. The electroplated surface is very clean and shows no contamination by copper. The traces of fluorine are negligibly small.

6Ir / Iridium

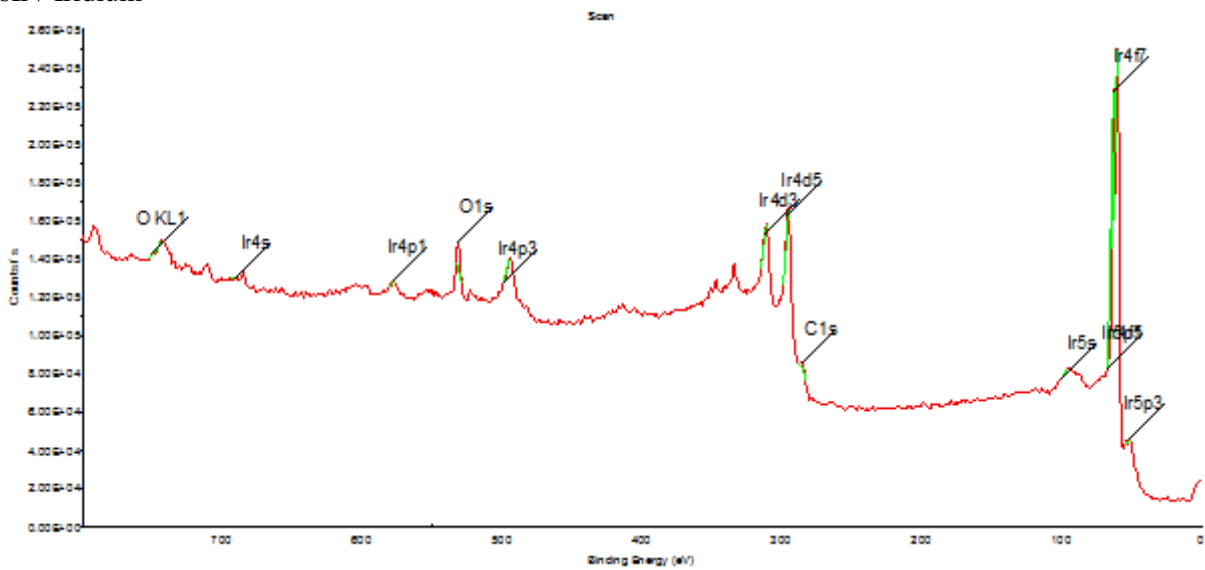


Figure 33: XPS spectrum of iridium sample. Iridium shows traces of Cu at 400 eV binding energy.

9AuPt alloy

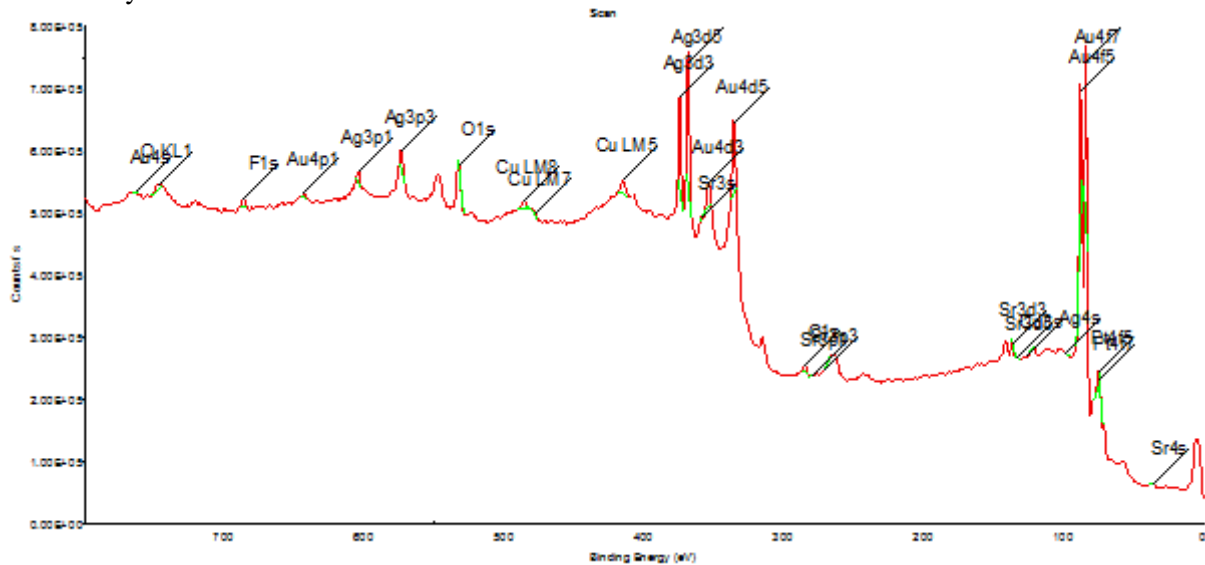


Figure 34: XPS spectrum of a AuPt alloy sample.

Note that the alloy referred to as AuPt should more properly be described as Au-Ag12-Cu9-Pt4 (% wt). In other words, it already contains significant amounts of copper and silver which are impossible to distinguish from contamination by the same elements from external sources.

6PtIr, alloy

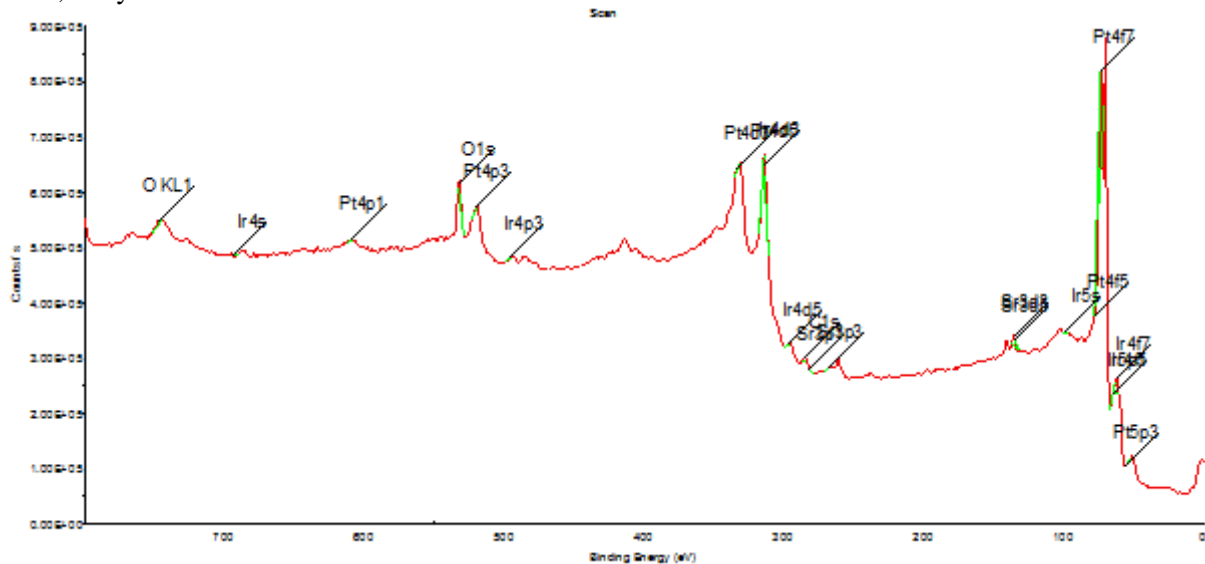


Figure 35: XPS spectrum of an PtIr alloy sample. The material also shows traces of Cu at 400 eV Binding energy.

4.2.3 XRF Measurements

For XRF measurements, only qualitative surface analysis could be performed due to the restricted sample size. Hence, X-ray fluorescence (XRF) analyses were carried out in conventional beam geometry in order to measure the level of trace contaminations in the bulk material. Here, qualitative results have

been derived from the X-ray fluorescence spectra. A quantification of the trace elements was not successful due to the unknown matrix composition, the quantitative determination of which would require beamline allocations (X-ray energies above 12 keV) as yet unforeseen for the project. A quantification of the surface contamination could not be achieved, because the samples size and surface roughness were not suitable to perform total reflection X-ray fluorescence (TXRF) analysis. The quantification of surface contamination requires a sample size of minimum length 20 mm and a surface roughness better 1 nm for hard X-rays and better than 4 nm for soft X-rays.

XRF measurements at higher incident X-ray energies (above 12 keV) could not be performed at the PGM and FCM beamline. Measurements performed at higher beam energies *e.g.* those available from the BAM beamline would be required to determine the bulk composition of the sample in a reliable way using L-fluorescence emission. For the measurements below 12 keV, the M-fluorescence lines have to be employed. Here the fundamental parameters (FPs) needed for the quantification are very unreliable and have high relative uncertainties. In table 8 we list all traces which could be identified by XRF. Selected spectra of these samples are shown in figures 36 to 39.

Table 7: XRF measurements performed at PTB's four crystal monochromator (FCM) beamline (1.75 – 10.5 keV) and plane grating monochromator (PGM) beamline (0.1-1.8 keV). Note* the measurements at the FCM beamline above 11 keV are in the regime of limited photon flux and spectral purity.

Sample		KMC beamline						Sample		PGM
		Energy / keV								Energy / eV
		8	10	11	11.4	11.7	11.99*			1622
7	PtIr		3600 s		3600 s		600 s	8	PtIr	600 s
10	AuPt	3600 s				3600 s	600 s	11	AuPt	600 s
7	Ir		3600 s				600 s	8	Ir	600 s
7	Si		3600 s				600 s	9	Si	600 s
7	W		3600 s	3600 s			600 s	8	W	600 s
		1.7e-7 mbar	repeated 3-4 times				repeated 6 times	1.8e-6 mbar		repeated 6 times

Measurements in grazing incidence geometry could not be carried out due to the small size and high surface roughness of the samples. In order to perform surface sensitive TXRF measurements a sample length of at least 20 mm and a surface roughness of 1 nm or better is required.

Table 8: Identified trace elements derived from XRF spectra. The most prominent fluorescence line is put in parentheses. For the trace elements marked in yellow, high fluorescence intensities have been found.

PtIr 7+8	AuPt 10+11	Ir 7+8	Si 7+9	W 7+8
C (K α)	-	C (K α)	C (K α)	-
N(K α)	-			N (K α)
O(K α)	O (K α)	-	O (K α)	O (K α)
-	-		F (K α)	-
Mg (K α)	-	-	-	Mg (K α)
Al (K α)	Al (K α)	-	Al (K α)	Al (K α)
-	-	-	-	-
-	-	Ca (K α)	-	-
Fe (K α)	Fe (K α)	Fe (K α)	Fe (K α)	Fe (K α)
Ni (K α)	-	Ni (K α)	Ni (K α)	Ni (K α)
Cu (L α & K α)	Cu (K α)	Cu (K α)	Cu (L α +K α)	Cu (K α)
Zn (L α & K α)	-	Zn (K α)	-	Zn (K α)
Ru (M α & L α)	-	Ru (M α & L α)	-	-
Ag (L α)	Ag (M & L α)	-	-	-

A quantitative determination of the surface contaminations requires TXRF measurements. The incident angle of the X-ray beam to the sample has to be tuned below the critical angle of total reflection. This ensures a low excitation of the bulk material and results in a high surface sensitivity. Typical angles are in the range between 0.2° and 0.9° for X-ray energies between 1.6 KeV and 12 keV and the width of the X-ray beam is usually 150 μ m to 500 μ m. This results in a required minimum of the sample length to project the beam onto the sample surface. Typically, a sample length of at least 20 mm is required to achieve this. In addition, the surface roughness of the samples should be better than 1 nm in order to ensure that total reflection occurs.

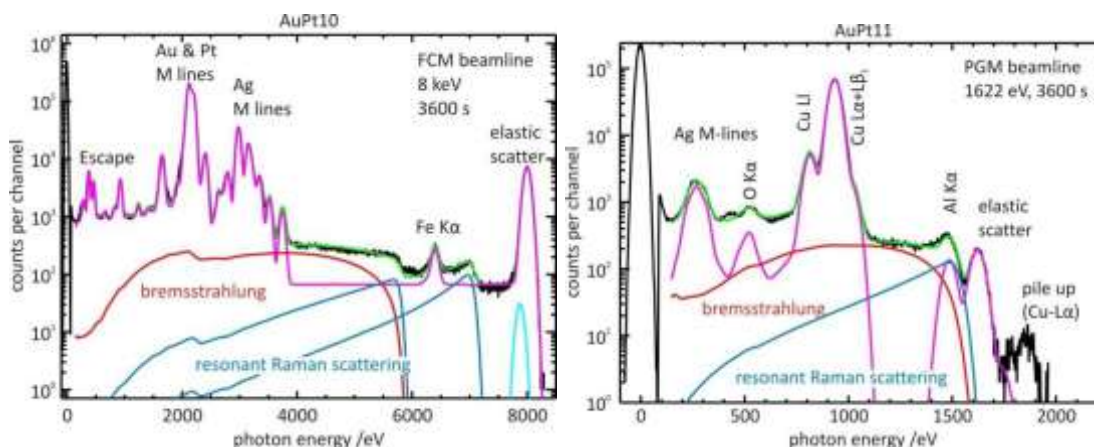


Figure 36: XRF spectra of the sample AuPt10 (left) and AuPt11 (right) measured at the FCM and the PGM beamline respectively. At the FCM beamline the exciting X-ray energy was tuned below the Cu K-absorption edge so as not to produce too high a count rate. At 10 keV the Cu K α and K β emission is very intense.

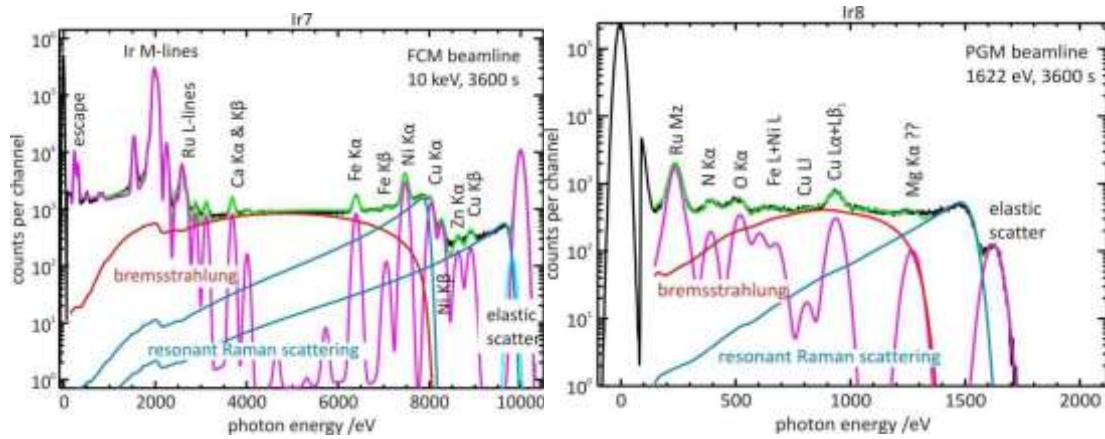


Figure 37: XRF spectra of the samples Ir7 (left) and Ir8 measured at the FCM and PGM beamline respectively. The element Ru was found in both spectra.

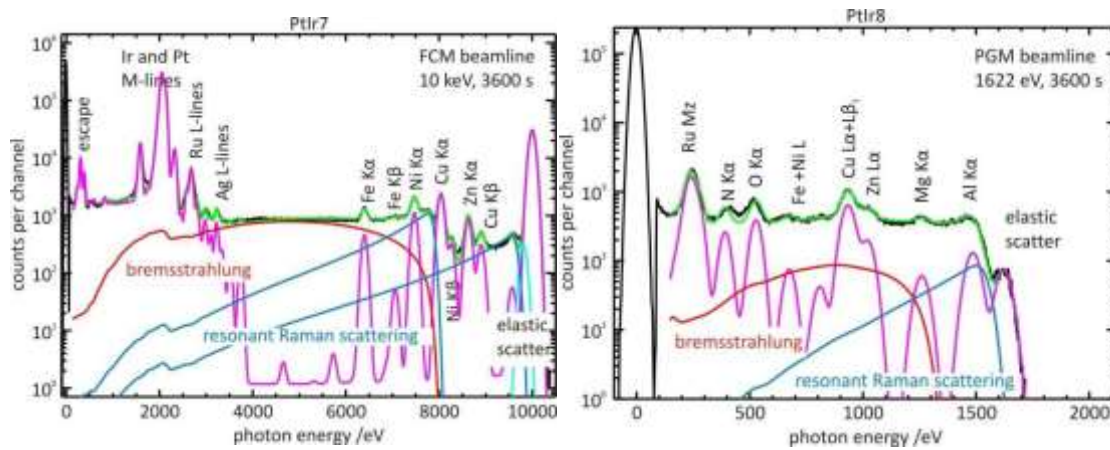


Figure 38: XRF spectra of the samples PtIr7 (left) and PtIr8 measured at the FCM and PGM beamline respectively. It seems that the Ru contamination is related to the matrix element Ir.

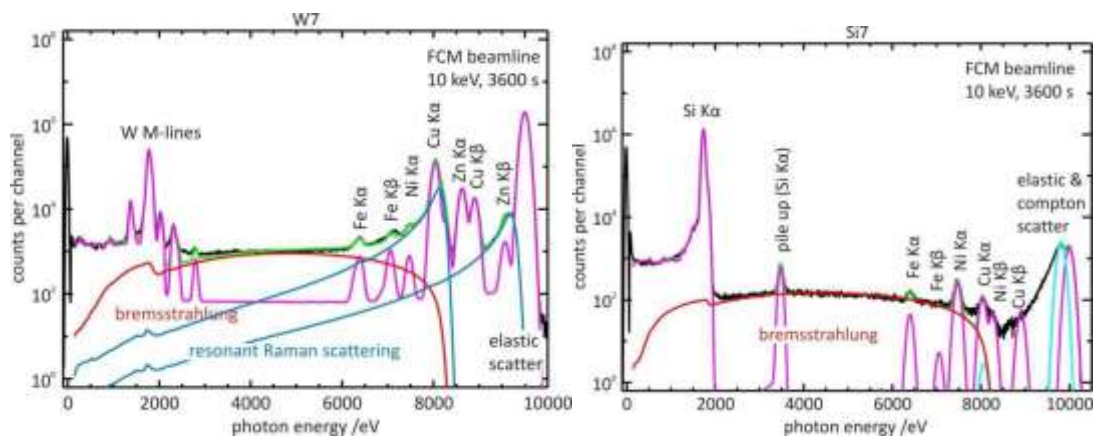


Figure 39: XRF spectra of the samples W7 (left) and Si7 both measured at the FCM beamline. Sample W7 shows a lot of transition metal contaminations, whereas the Si7 sample seems to be quite clean.

	C2 R1	1	C3 R1	2	C4 R1	3	C5 R1	4			
		9,91		9,88		9,90		9,92			
		9,10		9,07		9,09		9,11			
C1 R2	5	C2 R2	6	C3 R2	7	C4 R2	8	C5 R2	9	C6 R2	10
	9,90		9,89		9,91		9,86		9,89		9,86
	9,09		9,08		9,10		9,05		9,08		9,05
C1 R3	11	C2 R3	12	C3 R3	13	C4 R3	14	C5 R3	15	C6 R3	16
	9,92		9,85		9,87		9,87		9,91		9,89
	9,11		9,04		9,06		9,06		9,10		9,08
C1 R4	17	C2 R4	18	C3 R4	19	C4 R4	20	C5 R4	21	C6 R4	22
	9,90		9,88		9,88		9,85		9,93		9,90
	9,09		9,07		9,07		9,04		9,12		-0,81
											9,08940348
C1 R5	23	C2 R5	24	C3 R5	25	C4 R5	26	C5 R5	27	C6 R5	28
	10,01		10,00		10,00		9,96		9,95		9,94
	9,20		9,19		9,19		9,15		9,14		9,13
		C2 R6	29	C3 R6	30	C4 R6	31	C5 R6	32		
		9,93		10,00		9,98		9,95			
		9,12		9,19		9,17		9,14			

Figure 41: Resulting SiO₂ film thicknesses (nm) for the 10 nm (nom.) wafers.

The expanded uncertainty ($k = 2$) for the calibrated values is $U(d) = 1.0$ nm. The variation of the measured thicknesses varies from 0.23 nm (5-nm-wafer) to 0.16 nm (10-nm-wafer). Due to the given uncertainty a constant thickness value for both wafers may be assumed.

4.4 ROUGHNESS SURFACE CHARACTERISATIONS

CNAM used Angle Resolved Scattering to compare the surface roughness of three of the material samples under investigation. Figure 42 presents mean power spectral density (PSD) of each analysed sample. From these PSDs, the RMS height is extracted (see table 9). From the comparison of the PSDs, we can note that each material has a PSD of characteristic shape and amplitude. The PSD is a signature of the surface roughness in a given spatial frequency domain and provides information complementary to the RMS height values. The PSD amplitude is a good first indication of the roughness of the surface: silicon has a smoother surface than Udimet 720 and iridium.

The Udimet 720 and silicon PSDs present a quasi linear shape in the range $(0.1 - 2.7) \mu\text{m}^{-1}$ unlike the PSD for pure iridium. This might indicate that the mechanical polishing process, carried out using progressively smaller granularities at each step, does not allow one to reduce the asperities enough in the range $[0.15 - 1.2] \mu\text{m}^{-1}$. On the other hand, this may also be explained by the inhomogeneous metallographic structure of pure iridium observed using optical microscopy (figure 43).

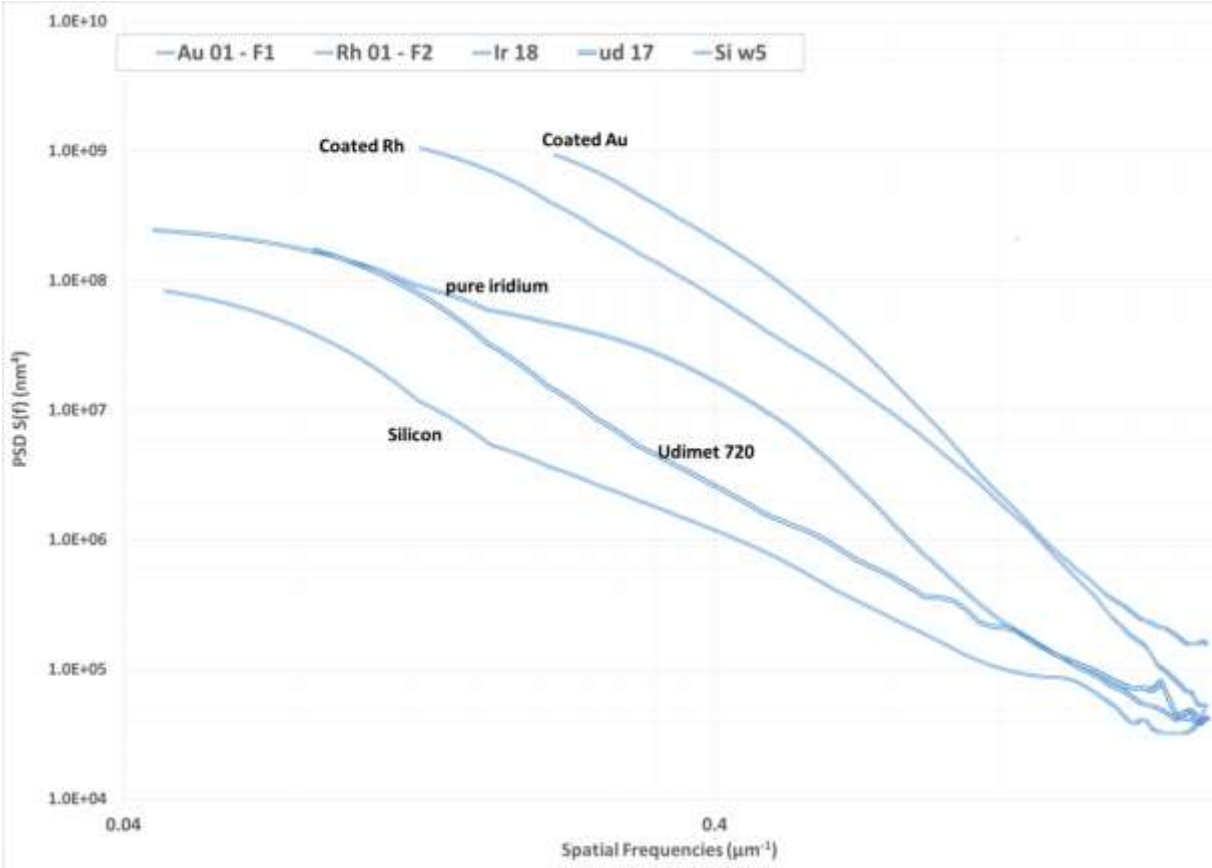


Figure 42: Mean power spectral density (PSD) curves for silicon, Udimet 720 and iridium (also shown are results from plated samples). Note: the units have dimensions of [L⁴] because the scattering is two-dimensional.

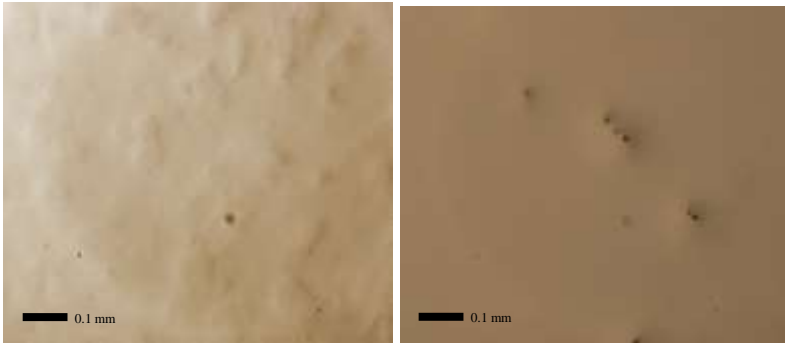


Figure 43: Optical microscopy. Left: pure iridium. Right: Udimet 720.

Table 9: Surface roughness (RMS) and uncertainty of samples measured as by Angle Resolved Scattering.

Sample Identification	RMS height / nm
Ir #16	4.0 ± 0.3
Ir #18	4.7 ± 0.1
Ir #20	5.0 ± 0.2
Ud #17	2.4 ± 0.4
Ud #18	2.4 ± 0.3
Si W0	1.6 ± 0.1
Si W5	1.7 ± 0.1
Si W10	1.8 ± 0.1

4.5 COMPARISON OF SURFACE ROUGHNESS BY COHERENCE SCATTERING INTERFEROMETRY

EJPD performed comparative measurements via CSI using a white light microscope ((image size $718 \mu\text{m} \times 546 \mu\text{m}$). Primary Profile Filtering used a noise filter Cut-off, at $\lambda_s = 2.5 \mu\text{m}$. Measurements were made according to ISO 4287 with a cut-off wavelength, of $80 \mu\text{m}$. The samples under investigation were cleaned using 3 cleaning techniques, BIPM *nettoyage-lavage* [3], UV Ozone [4] and H-plasma [5]. The results of the measurements are shown in figures 44 to 46. It should be noted that white light microscope measurements will, by the nature of the technique, heavily attenuate those special frequencies of less than $1.2 \mu\text{m}$.

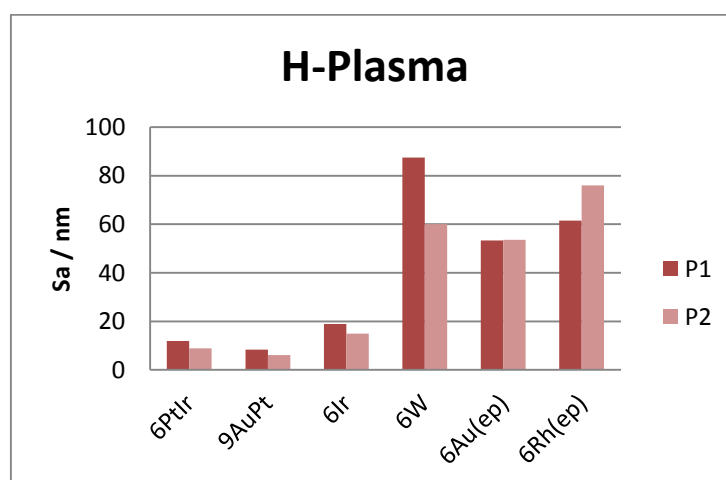


Figure 44: S_a surface roughness values for H-plasma cleaned samples (measurements taken at 2 positions, P1 and P2, on the sample surface).

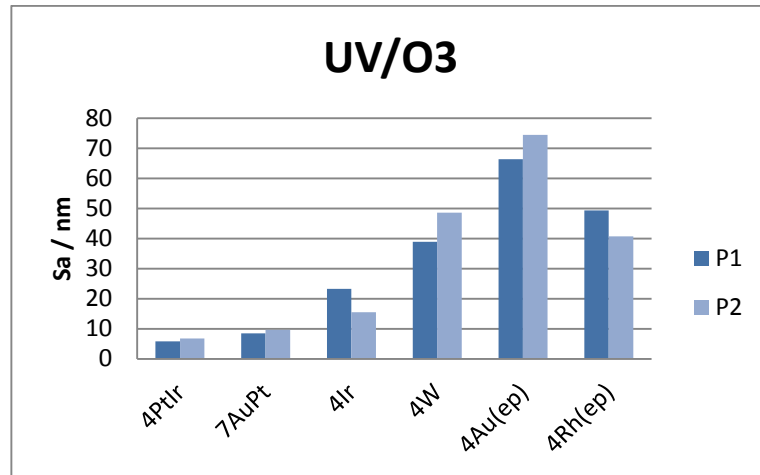


Figure 45: S_a surface roughness values for UV/Ozone cleaned samples (measurements taken at 2 positions, P1 and P2, on the sample surface).

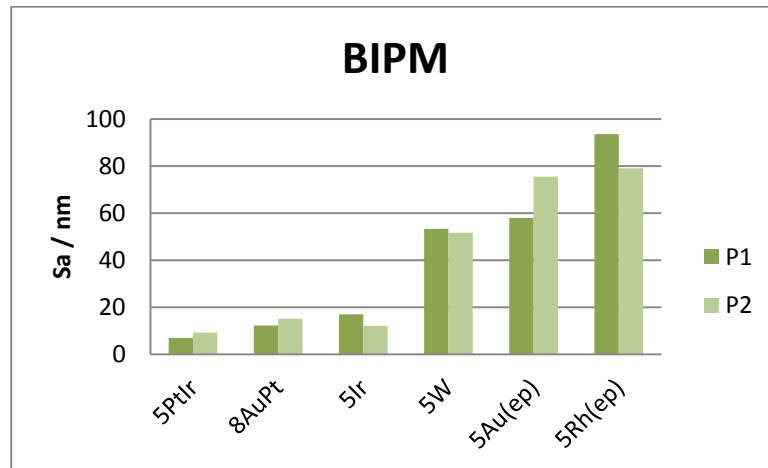


Figure 46: S_a surface roughness values for samples cleaned by *nettoyage-lavage* (measurements taken at 2 positions, P1 and P2, on the sample surface).

The results show broadly the same trends for the four uncoated materials tested with the exception of the tungsten sample. Surface roughness for the PtIr AuPt and Ir samples are of the order of 5 nm which is equivalent to the best finish achievable on weights made of metals or metal alloys (silicon mass standards and Avogadro spheres can be manufactured to a surface finish of 1 nm - 2 nm). The tungsten samples show a large variation on surface roughness; this is a function of the individual samples rather than the cleaning procedures used. Deep grooves were present over both tungsten samples 5 and 6 resulting in relatively high surface roughness values. The value obtained for tungsten sample 4 is more indicative of the underlying roughness achievable by polishing single crystal tungsten and is comparable with the finish on the other solid samples.

5 DISCUSSION

5.1 SURFACE ROUGHNESS

Table 10 summarizes the results of the surface roughness measurements performed with optical roughness meter, AFM and white light reflection method. Due to the variety of measurement techniques and the application data analysis methodology the results are not directly comparable. However, it is hoped that the range of surface measurement, viewed as a whole will present a coherent picture of the relative merits of the materials investigated.

The AFM roughness values (R_q) were obtained from the AFM images presented in section 4.1. The roughness values calculated from the larger AFM scans ($20 \times 20 \mu\text{m}$) were generally higher than the values acquired from the small area scans ($5 \mu\text{m} \times 5 \mu\text{m}$). The difference between these two values, taking into account sensitivity differences due to the scan size, may be interpreted as a measure of homogeneity. Generally, for a homogenous surface, the scan size should not significantly affect the roughness values given a constant AFM tip radius. From table 10 it can be seen that the effect of scan size was least for iridium, which was also found to be the most homogeneous surface in the AFM and SEM studies as there were no grooves or pits and very little contamination on the surface. It was also the smoothest surface based on AFM and SEM images and calculated roughness values. Platinum-iridium, iridium, stainless steel and tungsten also had surface roughness values of 10 nm and below, which is an indication of high quality surface finish.

The white light reflection method gave systematically higher surface roughness values for all studied sample materials. However, unlike AFM, it is not an absolute measurement method and therefore roughness values are only comparable with each other. The order of roughness for the materials studied is similar to the AFM results with iridium having the smallest roughness, but an exception was the value for the stainless steel surface which gave the highest roughness. A probable explanation is that white light reflection studies were made using the same samples as those used for SEM analyses. The SEM analysed stainless steel sample had more contamination than the AFM analysed surface, which could explain the relatively higher roughness value.

The optical roughness method, in the range $(0.1 - 2.7) \mu\text{m}^{-1}$ of the spatial frequencies, gave a higher roughness for iridium than silicon and Udimet 720 but all were of the same order so no firm conclusions can be drawn.

Table 10. Comparison of surface roughness results for the various methods used.

Sample material	Measurement Method				
	Optical roughness meter	AFM Scan size ($20 \mu\text{m} \times 20 \mu\text{m}$)	AFM Scan size ($5 \mu\text{m} \times 5 \mu\text{m}$)	White light reflection	White light microscope
	RMS ht. / nm	R_q / nm	R_q / nm	R_q / nm	Sa / nm
PtIr		9.9	5.7	12	10
AuPt					10
Ir	4.6	1.5	2.0	8	15
SS		4.6	3.2	54	
Si	1.7				
W		11.0	4.8	40	50
Ni (U720)	2.4				

5.2 SURFACE CONTAMINATION

Regarding surface contamination, all five materials measured by XPS yielded spectra of elements consistent with the materials from which they were taken. All of the survey scans showed that the surfaces of the five materials had both an oxide layer and a layer of hydrocarbon contamination. Small amounts of nitrogen were also identified in the survey scans and this is typical of samples that have been exposed to air.

Some of the samples showed trace amounts of chlorine and/or sodium. This was probably a result of a small amount of salt contamination on the surface coming from the environment. These trace amounts will have little effect on the surface properties of the samples and if desired could probably be removed by cleaning with a solvent.

The most interesting element identified in the survey scans was copper. The quantities detected varied from trace amounts (< 1%) in the Nickel-alloy and silicon samples to larger amounts (> 1%) in the tungsten, Pt-Ir and iridium samples. The XPS measurements made at 60° to the surface normal showed that the copper located in the bulk of the material below the hydrocarbon contamination and oxide layer on the surface of the samples. Therefore it is likely that this copper contamination is either a component of the substrate material or has formed on the substrate possibly as a result of the protocol used to polish the surface of the substrate.

As opposed to the XPS measurements, the determination of the surface contaminations in mass per unit area could not be performed successfully with XRF due to the limited surface sensitivity of the (conventional) XRF technique. However, a qualitative evaluation of trace elements in the bulk was successfully achieved. Table 8 lists all traces which could be identified by XRF. Most of the identified trace elements are probably in the range of 10^{-3} or less weight fraction. Exceptions are silver and copper in samples AuPt10 and AuPt11, Ru in samples Ir7, Ir8, PtIr7 and PtIr8 as well as copper in samples W7 and W8. Here, the weight fractions are probably in the percent range. The amounts of copper and silver in the PtIr samples seem to be of the order of a matrix component. Selected spectra of these samples are shown in figures 36 to 39. A quantification of the traces in the bulk was not possible owing to the high relative uncertainties of the relevant FPs for M-fluorescence emission. In addition, the bulk composition of the samples (main matrix elements) was not known, which could have helped to provide at least a reliable estimate of the initial trace concentrations in the bulk.

6 CONCLUSION

Nine different materials were examined as candidates for mass standards to be used in watt balance experiments and for the conservation of the mass unit: platinum iridium alloy, pure iridium, tungsten, a gold-copper-platinum-silver alloy, stainless steel, Udimet 720 (a nickel based superalloy), silicon and copper electroplated with gold or with rhodium. Of these, PtIr is the material from which the international prototype and national primary kilogram standards have been produced. With respect to PtIr, tungsten and iridium are comparably dense but harder and have lower magnetic susceptibilities. Stainless steel is the metal from which most secondary kilogram standards are made. Udimet720 has similar density but is much harder and has a lower magnetic susceptibility. However, it cannot replace stainless steel for secondary standards because its density is not exactly the same. Silicon is important because it lies at the heart of the International Avogadro Coordination. Bulk copper has a very low magnetic susceptibility, can be pure but is too soft and chemically reactive to be used for mass standards. Electroplating has been used to produce samples with harder, inert surfaces. Such electroplated samples have been evaluated as part of a separate study [6].

The properties of the materials studied were surface roughness at different distance scales using a variety of techniques (laser scattering, atomic force microscopy, white light scattering), hardness and contamination. For silicon, samples were produced with a natural oxide layer, as well as 5 nm and 10 nm thick oxide layers.

Surface studies using optical roughness meter, SEM and AFM show that all studied materials have a relatively smooth and homogenous surface. Roughness values (R_q) of 10 nm or less were obtained for platinum-iridium, iridium, stainless steel and tungsten. Roughness measurements using white light reflection support these findings. AFM and SEM studies were performed with different samples of the same materials. The results of the two methods were qualitatively similar, except for stainless steel and tungsten. The AFM analysed samples had grooves not found on the SEM analysed samples which is probably due to the relatively poorer resolution of SEM for this application. All materials analysed at MIKES were found vacuum compatible as no surface damage was observed due to ultra-high vacuum exposure during SEM studies.

Surface contamination measurements performed both by XPS and XRF also led to similar results with a copper contamination on all tested material. The presence of this element is certainly due to the polishing procedure as all surfaces, except Si samples, were mechanically prepared. Providing the copper contamination is stable then there is no issue with the minimal presence on the materials and the experiments with the surface samples in WP3 and WP4 of this JRP can continue as planned. However, it may be worth investigating the reason behind the copper contamination with a view to reducing/eliminating it from the preparation of mass standard artefacts.

One of the principal aims of the present study was to identify the best candidate materials for the realisation and dissemination of the mass unit. Pure iridium samples showed a good surface finish (roughness < 5 nm, good visual appearance after polishing and low surface contamination). Given in addition its low magnetic susceptibility compared with platinum iridium alloy, the material appears to be a good candidate for a watt balance experiment. However, its hardness makes it very difficult and time consuming to polish and it is quite difficult to get high quality pure iridium.

Similarly tungsten has good mechanical and magnetic properties. The samples used for this

Silicon samples had the smoothest of all surfaces (roughness < 2 nm). This material has already been used in the NRC-CNRC watt balance and, of course in the International Avogadro Coordination. It is easier to produce spherical artefacts than cylindrical ones because the material is brittle. Extensive ongoing work on silicon artefacts has been performed by the International Avogadro Coordination. However, the studies carried out by this JRP have been on plane surfaces and so are complementary to this work.

By contrast, some materials are clearly disfavoured. Aside from its low magnetic susceptibility, the gold-platinum-silver-copper quaternary alloy shows few advantages; it also turns out to be difficult to reproduce samples of identical composition. As for copper samples electroplated with gold or rhodium, the surface is inhomogeneous but this could be related to the condition of the underlying substrate. It is suggested that substrates be characterised prior to coating if future samples are produced.

REFERENCES

- [1] Shipping document. NewKILO WP1.
- [2] C. Zerrouki, F. Miserey, and P. Pinot, “Light scattering angular distribution of a mirror-polished CoCr20WNi (alacrite XSH); application to the determination of statistical parameters characterizing the surface roughness,” *Eur. Phys. J. Appl. Phys.*, 1, pp. 253–259, 1998.
- [3] G. Girard, “The Washing and Cleaning of Kilogram Prototypes at the BIPM” (Sèvres: BIPM) (1990).
- [4] K. Marti, P. Fuchs and S. Russi. “Cleaning of mass standards: a comparison of new and old techniques”, *Metrologia*, 49,628 (2012).
- [5] J. Berry, S. Downes and S. Davidson. “UV/ozone cleaning of platinum/iridium kilogram mass prototypes”, *Metrologia*, 47, 410 (2010).
- [6] EMRP SIB-05 DELIVERABLE 1.2.2 HOMOGENEITY AND RESISTANCE OF METAL ON METAL COATINGS

ACKNOWLEDGEMENTS

The work leading to the results described in this publication is part of the European Metrology Research Programme (EMRP), which is jointly funded by the EMRP participating countries within the European Association of National Metrology Institutes (EURAMET) and the European Union.